AN INVESTIGATION OF THE PROPERTIES OF NEW SEMICONDUCTING ALLOYS AND THEIR APPLICATION TO LUMINESCENT DEVICES

Final Technical Report on

National Aeronautics and Space Administration

Grant No. NGR 40-002-094

September 13, 1970 - June 30, 1971

by

Maurice Glicksman and Aaron Wold

Division of Engineering

Brown University

Providence, Rhode Island

August 6, 1971

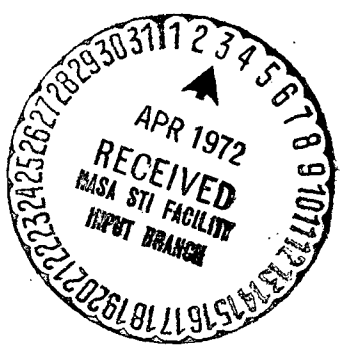

PAGES-65

CAT. 26

ABSTRACT

Crystals of alloys of GaP with ZnSe have been grown with ZnSe contents up to 8 mol percent. Study of the transport properties of n-type samples of such alloys showed a hopping contribution to the conductivity at low temperatures, and the dominance of ionized impurity scattering above about 150 K. The electron mobility decreased with increasing ZnSe content. The hopping mechanism was found to have an activation energy at low temperatures of about 4 meV, for all of the alloys studied. Cathodoluminescent studies of the alloys showed no signs of Zn-Se donor-acceptor pair recombination. Diodes fabricated from the alloy material (by the diffusion of Zn as an acceptor impurity) showed electroluminescence at room temperature (and below), although weaker than that found from GaP diodes by as much as two orders of magnitude. For the more heavily alloyed diodes, line spectra were not seen near the band edge; in the reverse bias direction, the emission did tail out to higher energies than seen in the pure GaP diodes. Indentifiable pair-recombination emission in the alloy diodes showed a slight decrease in energy with alloying, from 1.95 to 1.91 eV on going to 5% ZnSe, for what was tentatively identified as a Si-Si pair recombination or a Si-S pair recombination line, in pure GaP. The line may involve Se in the alloys, and the shift may be in part chemical. Success in the growth of single crystals of this quaternary alloy system should allow further study of the alloy optical properties, at greater alloying concentrations.

I. Introduction

Very little has been known of the optical and electrical properties of alloys of III-V with II-VI compounds. Recent investigations[1-5] have shown that several compounds do form alloys over the whole range of composition, namely, GaP-ZnSe[2], GaAs-ZnSe[2,4], and GaP-ZnS[2,5] and the dependence of the energy gap upon composition has been determined for the above three systems at room temperature. The property of a continuously variable energy gap should permit control of the spectra of radiation-emitting diodes. The absorption measurements[2] showed possible evidence for a transition from indirect to direct recombination in the GaP-ZnSe alloys systems; direct recombination is expected to be an important condition for highly efficient radiation recombination to take place. These direct band-gap materials may satisfy the need for high efficient and visible light-emitting diodes, if it is also possible to make p-n junctions of low resistance.

Of three alloys system the system GaP-ZnSe was chosen as the first to investigate because of large band-gaps in the range 2.15-2.6 eV (at room temperature) and the known luminescent properties of GaP[6], which is the most promising visible light-emitting diode material. More information is also available on the electrical properties of that system[7].

Thus this research is aimed at producing good quality crystals of these compound alloys, studying the dependence on composition of the luminescent and electrical properties, using the materials to make junction devices, and studying their electroluminescence. Crystals of GaP and alloys in the range up to 8 mol per cent ZnSe have been grown; their electrical, cathodoluminescent and electroluminescent properties are presented in this report.

II. Growth of Crystals

Crystals of the system GaP-ZnSe and GaP were grown by either of two techniques, i.e., chemical transport[8] using iodine as the transport agent, or crystallization from a gallium melt.[9]

A. Solution Growth of GaP and GaP-ZnSe

Platelet type crystals of GaP and GaP-ZnSe in sizes up to 2 × 3 × .5mm thick have been grown in a solution of liquid gallium. The technique used to prepare and grow these crystals is as follows:

A 10 gram slug of 99.999% pure gallium (obtained from Alussisse Metal Inc.) is placed in a 9 mm I.D. quartz tube. The tube was cleaned with 20% solution of HF, rinsed with distilled water, and torch-dried under vacuum. The loaded tube is then outgassed at 5×10^{-5} torr. To ensure maximum outgassing, the gallium is torch-heated to a cherry red color. The tube is then allowed to cool, the vacuum is broken, and the charge material is added in pulverized form. (It was found that the best crystals grew when a ratio of 10 grams of gallium to 0.7 grams of charge material was used.) The sample is then returned to the vacuum system for final evacuation and sealed. A Harper furnace is used to heat the capsule to 1200°C. After allowing an equilibrium period of three hours, the sample is then cooled to 800°C at a rate of 5°C per hour. Crystals are removed when cool and boiled in a 20% HCl solution to remove any remaining gallium. The GaP used in these experiments was obtained from the Monsanto Chemical Co., and the ZnSe was grown by chemical transport using iodine as a transport agent in the Brown University Materials Preparation Laboratory.

There were difficulties in the analysis of the ZnSe content in the case of crystals with low concentration of ZnSe. In addition to questions about the accuracy of determination (made by emission spectroscopy, atomic absorption and X-ray lattice determination), there were observed variations of the content among crystals grown in the same tube. There was sufficient corroboration, however, to show that samples grown from gallium solution were much lower in ZnSe content than the original charge--this was down by more than a factor of 10 in some cases. The difference between charge and crystal compositions for materials grown with iodine transport was much smaller, being generally only a factor between 1 and 2. On this ground, emphasis was put on the vapor transport method to grow crystals, expecially since our objectives were set for higher contents of ZnSe.

B. Growth of GaP and GaP-ZnSe by Chemical Transport

In the techniques of chemical transport, as applied to GaP and the GaP-ZnSe system, crystals are grown by transport through a temperature gradient using iodine as the transport agent.

The charge material is prepared by firing the high purity elements, along with 5 mg. of iodine as a mineralizing agent, in silica tubes evacuated to 10^{-3} torr. After approximately 10 days of reaction at 1000°C, the tubes are cooled, opened, and the compound boiled with 20% HCl to remove any unreacted elements. The compounds are then carefully washed with distilled water and vacuum dried.

A one gram charge of the desired composition is placed in the filling apparatus, which is evacuated to 5×10^{-5} torr. The iodine is introduced, and the transport tube sealed off. An iodine concentration of 8 mg/cm^3 is used. The tube is placed in the transport furnace, and back transported for 24 hours to remove any charge powder from the walls of the tube, where growth is to take place. The temperature of the furnace is then raised to 1000°C and after equilibrium has been reached, a temperature gradient of 25°C is created in the growth zone by cooling the zone at an average rate of 1°C/hr.

Crystals of the system GaP-ZnSe with concentration of up to 16% (wt.) ZnSe have been grown with this technique. Crystals as large as 2 × 2 × 3mm were grown. Determination of the concentration of the ZnSe was done from X-ray diffraction measurement of the lattice constant, and the application of Vegard's law for crystals of higher than 5% ZnSe content. X-ray analysis also enabled a test of the homogeneity and phase of the material.

III. Electronic Transport Properties

There have been several reports of measurements of properties of (III-V)-(II-IV) alloys: one[7] of the alloy $(GaP)_{.95}(ZnSe)_{.05}$, another[10] of InAs-rich alloys in the InAs-ZnSe system, and a third[11] of alloys in the InAs-rich end of the InAs-CdTe system.

An interesting feature of the (III-V)-(II-VI) alloy system is the fact that the compounds are not expected to fit into each other's lattice bonding arrangement without charge compensation taking place. The Zn and Se atoms are known acceptors and donors, respectively, in pure GaP, but the Zn and Se can be substitutional acceptor and donor or they might be donor-acceptor pairs (locally compensated) in the GaP-rich GaP-ZnSe alloys system. The locally compensated donor-acceptor pairs should scatter electrons differently than do random donors and acceptors.

Another feature of interest is related to impurity banding effects. If there are impurities not associated with the dipolar pairs those impurities could act as donors and acceptors. If the Zn and Se atoms acted as impurities in the GaP-rich GaP-ZnSe alloys, for 1% of ZnSe there would be 2.47×10^{20} atoms/cm^3 of Se or Zn. The ratio of the average donor distance r_D $[=(3/4\pi N_D)^{1/3}]$ to the effective radius of a hydrogenic donor a_o $[=(m_o\varepsilon/m^*)a_H]$ is less than 1. N_D is the donor concentration, ε the dielectric constant, m^* the effective mass and a_H the hydrogen atom Bohr radius (0.53 Å) Consequently impurity banding would be expected.

Mostly, rectangular samples were made from the crystals grown and polished down to flat dimensions. A typical size was 1.5 x 0.6 x 0.01 mm. Ohmic contacts were made by alloying In-Ga (0.5%) dots (of 0.1 ∿ 0.2 mm

diameter) at the edges of samples under a hydrogen atmosphere, in the temperature range 400 ∿ 500°C for 5 ∿ 10 minutes. Contacts to the dots was made by ultrasonic bonding with 1 mil Au wire. For Hall coefficient measurements an ac method was employed with a 6000 gauss magnetic field, where the appropriate bucking circuit was used with a Princeton Applied Research lock-in amplifier (HR-8). The Hall coefficient R_H was found to be independent of magnetic field up to 6000 gauss. Resistivity measurements were made dc, with a Leeds and Northrup K-3 potentiometer. The measurements were made in the temperature range 8 ∿ 360°K and the Hall coefficient and the sign of the Seebeck coefficient verified that the materials were n-type even though most samples were not intentionally doped. Table I gives information on the material from which measured crystals were taken.

A. Resistivity and Hall Coefficient

Fig. 1 summarizes the resistivity measurements of several samples of the alloy crystals available and Figs. 2-6 show the resistivity of different samples, together with their Hall coefficients. As suggested by Fritzsche[12] the temperature dependence of the resistivity ρ may be represented by

$$\rho = c_1 \exp(\varepsilon_1/kT) + c_2 \exp(\varepsilon_2/kT) + c_3 \exp(\varepsilon_3/kT) \qquad (1)$$

where ε_1, ε_2, and ε_3 represent activation energies. The energy required to activate electrons into the conduction band is given by ε_1 and is related to the thermal ionization energy E_D. In the range where ε_3 is observed, conduction occurs through electron hopping from occupied to unoccupied donors with the aid of phonons[13,14].

From the curves of the resistivity vs. the inverse of temperature two kinds of activation energies ε_1 and ε_3 may be usually inferred. Table II lists values of ε_3 for various samples; the range of change of ρ or n was too small to yield reliable values for ε_1, although estimates in the range 26-30 meV could be made. We see that $\varepsilon_3 \approx 4$ meV. In all the samples measured (see Figs. 3-6), a broad maximum in the Hall coefficient, the existence of which is well known as the harbinger of impurity conduction[13], is observed in the temperature range where the transition between the two kinds of activation energies occurs in the $\rho(T)$ curves.

The activation energy ε_3, related to possible hopping conduction, is observed below temperatures of $30 \sim 25°K$, where the Hall coefficient measurements could not be made. The other activation energy ε_1 is observed above the temperature $130 \sim 150°K$ even though the range of change of ρ is small. ε_1 should be related to the impurity ionization energy and should decrease with increase of impurity concentration, although the concentration dependence is not well understood. Our measurements $\rho(T)$ indicate that ε_1 probably does not decrease with increasing content of ZnSe (up to 5%) in the alloys. We know the variation of optical band gap[2] with alloy composition at room temperature in this system, but the detailed difference of band structure between pure GaP and the alloys is not known.

The n-type "doping" could be due to other unknown impurities, or to excess Se (non-stoichiometry of the alloy). The values of ε_1 may not be decreasing with alloy content because of the relatively large density, which varies from sample to sample, which may represent a saturation level of doping of Se. However, the values of ε_1 are too

uncertain to draw conclusions (by comparing with the density n, for example) on this question.

The Hall coefficient R_H increases with decreasing temperature for temperatures higher than 130 $\sim$ 150°K and has the broad maximum which indicates a transition to hopping conduction. If the Hall-to-drift mobility ratio is assumed as unity, the electron concentrations were in the range $3 \times 10^{17} \sim 5 \times 10^{18}$ cm^{-3} at the temperatures measured.

B. Mobility

Fig. 7 summarizes the Hall mobility R_H/ρ as a function of temperature. As our measurements on GaP show, typical values of the electron mobility at room temperature[15-17] in relatively pure GaP in which the carrier concentration is about 10^{17} cm^{-3} are 100 $\sim$ 200 $cm^2/Vsec$ and the mobility shows a $T^{-3/2}$ dependence in the temperature range above 100°K. This temperature dependence was analysed in terms of optical phonon scattering, the combination of optical and acoustical phonon scattering, or the combination of the acoustic phonon and intervalley scattering. Impurity scattering due to an (unknown) density of impurities is also present.

In the alloy system, however, the mobility is a monotonically increasing function of temperature over the temperature ranges of 50 - 360°K, even though the mobility of samples of low ZnSe content appears limited by phonon scattering at high temperatures. As the content of ZnSe is increased the mobility is reduced down to 7 cm^2/V - sec in the alloy $(GaP)_{0.95}(ZnSe)_{0.05}$ at room temperature. This behavior of the mobility immediately shows evidence of the dominance of ionized impurity scattering[18,19]. Even though the validity of the Born approximation may

not be good at low temperature with high concentration of carriers a calculation of the ionized impurity scattering has been carried out with the measured electron density. In the calculation we have assumed that electrons in the alloys have almost the same properties as those in pure GaP with the following parameters: dielectric constant $\varepsilon_\infty = 9.09$ and $\varepsilon_S = 11.1$[20] at 300°K. and an electron effective mass $m^* = 0.37\ m_o$[21]. The electron screening was treated by Dingle[19].

$$\mu_I = \frac{2}{3}\frac{e}{m^*}\frac{1}{F_{1/2}(\eta)}\tau_1^o e^\eta \int_o^\infty \frac{x^3 e^{-x} dx}{[\ln(1+Ax) - \frac{Ax}{1+Ax}](1 + e^{-x+\eta})^2} \qquad (2)$$

where,

$$\tau_1^o = \frac{\varepsilon^2 (2m^*)^{1/2}(k_B T)^{3/2}}{\pi e^4 N_I}$$

$$x = \frac{E}{kT} \quad , \quad \eta = \frac{E_F}{kT} \quad , \quad A = \frac{2\varepsilon m^* (k_B T)^2}{\pi e^2 \hbar^2 n^*}$$

and

$$n^* = n + (n + N_A)(1 - (n+N_A)/N_D)$$

Integration over the electron energy distribution was done by computer for the appropriate Fermi distribution. The calculated ionized impurity scattering gives a temperature dependence weaker than $T^{3/2}$ (see Fig. 8). The decreased temperature dependence observed at higher temperature could be interpreted as the result of a combination of impurity, phonon and dipole scattering. This will be discussed later.

The stronger dependence of mobility on temperature at temperatures below 130°K, down to 50°K, can be considered as the result of the possible beginning of hopping conduction between localized states in the impurity band. In the temperature range of 150-40°K the transition between two activation energies appears in the resistivity, and the broad

maximum of the Hall coefficient appears. This fact explains the sharp decrease of mobility due to hopping conduction, which could not be fitted with the ionized scattering.

Figs. 9 and 10 present the mobility vs. the inverse of temperature. The fact that the mobility can be expressed as an exponential with an activation energy below temperatures of 130-150°K also indicates that an (impurity) hopping mechanism is involved in this region. Table II shows the mobility activation energy calculated.

A calculation of the combined impurity, acoustic phonon and dipole scattering was made to explain the decreased temperature dependence of the mobility at high temperatures. The mobility can be expressed as

$$\mu = \frac{e\langle\tau\rangle}{m^*} \tag{3}$$

where

$$\frac{1}{\tau} = \frac{1}{\tau_a} + \frac{1}{\tau_I} + \frac{1}{\tau_d}$$

τ_a , τ_I and τ_d are the relaxation times due to lattice, ionized impurity, and dipole scattering, respectively. τ_a[22] , τ_I[19] and τ_d[23,24] are defined as follows;

$$\tau_a = \frac{\pi k^4 \rho u_\ell^2}{2^{1/2} E_1^2 m^{*3/2} (k_B T)^{3/2}} x^{-1/2} \quad , \tag{4}$$

$$\tau_I = \tau_I^o \frac{x^{3/2}}{F(x)} \quad , \tag{5}$$

where

$$F(x) = \ln(1+Ax) - \frac{Ax}{1+Ax} \quad ,$$

$$\tau_d = \frac{6\epsilon^2 \hbar^2 (k_B T)^{1/2} x^{1/2}}{2^{7/2} R^2 e^4 m^{*1/2} N_d} \frac{1}{G(x)} \tag{6}$$

where

$$G(x) = \frac{2 + x/r^2}{1 + x/r^2} - 2\frac{r^2}{x} \ln\left(1+\frac{x}{r^2}\right) \quad ,$$

$$r^2 = \frac{\pi \hbar^2 e^2}{2m^* \epsilon k_B^2} \frac{n}{T} \quad .$$

ρ is the density of the solid, u_ℓ is the velocity of longitudinal sound waves, and E_1 is the deformation potential averaged over direction in k-space. The density of GaP (4.13 g/cm^3) was used for the alloys. u_ℓ is[25] 6.15×10^5 cm/sec for GaP. The dipole scattering law is employed with the assumption that the distance R between atoms in the dipole pair is the nearest neighbor distance in the GaP lattice (R = 2.3601 Å).

Integration over the electron energy was done in the same way as for the calculation of ionized impurity scattering. The value of the deformation potential constant E_1 in the acoustic scattering is an open question for GaP. This value is fitted to the experimental mobility curve with a certain number of ionized impurities and dipole density, assuming that the sample is a 0.5% ZnSe alloy. This gives a deformation potential constant E_1 of 27 eV. As we see from Fig. 8 the value gave a good fit to the measured mobility curve of one of the GaP samples for temperatures above 130°K. Fig. 8 shows the mobility due to acoustical phonon, dipole, ionized impurity scattering, respectively, and also the combined mobility including the above mechanisms.

It is evident that the dipole scattering doesn't contribute to the mobility for the samples of low ZnSe content. But it is expected that the dipole density increases as the concentration of ZnSe goes up and the dipolar pairs contribute rather weakly to the scattering. Measurements on high content ZnSe samples are needed to evaluate the contribution of the dipole scattering to the mobility. Also it is noted that the alloy

scattering, important[26] in the alloy system Ge-Si, and not in $GaAs_{1-x}P_x$ and most other III-V compound alloys, was not observed in the composition range of our alloy system measured. Because of the strong impurity scattering, and low carrier mobilities, it is not expected to be important in this system.

IV. Cathodoluminescent Properties

It is desirable to know what kind of recombination centers are present in the alloy system before junction devices are made from these materials. Since the change from indirect to direct band gap in the GaP-ZnSe system is believed[2] to occur at a composition of around 25% ZnSe, all observed recombination at lower composition is believed to be related to impurities and imperfections. GaP exhibits a number of below band-gap radiation transitions, i.e., acceptor-pair recombination,[28] exciton recombination at isoelectric impurities,[29] exciton recombination at nearest-neighbor donor-acceptor complex,[30,31] free-to-bound carrier radiative recombinations,[32-34] and internal radiative transition at impurity centers.[35]

Some photo- and cathodoluminescent investigations were made on (III-V)-(II-VI) alloys: some alloys of the GaP-ZnSe system,[2,3] alloys of GaP-ZnSe,[5] in which the dependence on composition of the maximum in emission was found to be similar to that of the band-gap variation, and some alloys of the ZnSe-AlP[36] system.

As we know from the electronic transport properties of the alloys of GaP-ZnSe system, impurity banding is present. It is therefore anticipated that banding effects influence the radiative recombination properties. The intensity reduction of S-C donor-acceptor pair luminescence and of Bi-bound-exciton luminescence due to the excess concentration of neutral sulfur in GaP was explained with an impurity banding Auger model by Tsang, et al.[37] The concentration quenching of the luminescence from Zn-O complexes with increased Zn content in GaP is also

known.[38,39] An absorption experiment[40] showed that strong doping caused the "C" line due to Te to disappear in the absorption spectrum of a sample of GaP doped with Te to $n = 9 \times 10^{18}$ cm^{-1}. Recently Sinha and diDomenico[41] explained that the concentration quenching of bound exciton luminescence, especially for the Zn-O bound exciton in GaP, was caused by majority carrier screening and Auger mechanism.

For cathodoluminescence studies a thoriated tungsten T.V. electron gun under 10^{-5} torr vacuum was used with Bausch and Lomb #33-86 monochromators. A liquid nitrogen-cooled PbS cell was the detector with the proper chopping system. The power used was $1 \sim 20$ μA at 15-20 kV. The measurements were usually made at liquid nitrogen temperature.

Table III and Fig. 11 summarize the cathodoluminescent properties at 77°K for the samples of GaP and the alloys up to 8% ZnSe.

A. "Si-doped" Samples

Samples 615G-4, 625GZ-10, and SG61-2 show peaks in luminescence at 1.95eV, 1.92eV, and 1.91eV. All these samples were grown from gallium solution. Other studies[42,43] on Si-doped samples yield lines at this (GaP) energy, and so would indicate that our samples are doped unintentionally with Si. Even though the electronic transport measurements on one sample of the same lots were made, it was difficult to decide from them what material acts as the n-type dopant. Therefore, the 1.95eV peak may be due to Si-Si or Si-S (because the starting material does not contain Se and Te as residual impurities). The other peaks at 1.92eV and 1.91eV can be considered a Si-Si, Si-S, or Si-Se. The energy

shift to lower energy with the increase of ZnSe content could be due to the broadening of the impurity band. Then, the recombination could be from the bottom of a Se impurity band.

B. Iodine Transported Samples

Samples 31270-100, 927CT-6, and B430CT-1 were grown by vapor transport with iodine. Sample 31270-100 (GaP) has two peaks at the energies of 1.62eV and 1.01eV. Bhargava[44] observed luminescent peaks of 1.73eV and 1.69eV at 77°K which were tentatively attributed to deep donor (like Cl, I) and shallow acceptor pair recombinations, but the peaks were rapidly quenched above 100°K. A 1.69eV emission peak was found in the electroluminescent spectra of GaP doped with Te[45] and Te,Si.[46] Those were analyzed as due to Te and red phorphorus micro-occlusions[46] independent of the dopant. Our 1.62eV peak at liquid nitrogen temperature shifts to lower energies with increase of temperature and is seen even at room temperature.

C. Quenching of Pair Recombination Due to Zn and Se

Sample SG77-5 doped with sulfur shows emission at an energy of 2.14eV. This emission may be considered as sulfur-cadmium donor-acceptor pair recombination.[28] Sulfur and cadmium are deeper donors and acceptors than are Zn and Se. We do have Se and Zn in the alloys, but the pair recombination involving Zn and Se is not observed in the alloys. Even though the red luminescence due to Zn-O is present (but weak) in the spectrum of the alloy diodes (doped with Zn to make the p-type region; see next section), the radiative recombination due to the Zn-O complex is not observed in cathodoluminescence.

As we see from the Si-associated emission of the alloy samples, donors are possibly forming an impurity band but acceptors (Si) are not forming an impurity band. The electron level in the Zn-O exciton is deep; however, the hole level is in a zinc impurity band. But Se and Zn respectively could form impurity bands. These impurity bands could be responsible for the quenching of pair luminescence involving Zn and Se.

V. Electroluminescence

Considerable effort has been made to increase the efficiency of visible light emitting diodes. Recently external quantum efficiencies up to 7.2×10^{-2} and 6×10^{-3} have been reported for red-emitting GaP:Zn-O[47] diodes and green electroluminescence in GaP:N.[48] For (III-V)-(II-VI) alloys room temperature visible light-emitting junction diodes[49] were reported to have been made by forming a p-type doped mixed alloy of II-VI with "small" percentage III-V (GaP) material on an n-type II-VI substrate. The n-type substrate was either a zinc sulfo-selenide mixed crystal or zinc sulfide.

We have prepared junction devices from the samples listed in Table I. The samples were lapped down to flat dimensions and polished with 0.3μ alumina powder. The samples were briefly etched in a hot solution of $HCl:HNO_3$ (1:1) and sealed under a vacuum of $\sim 10^{-3}$ torr in cleaned 5 × 7mm quartz tube. The volume was about 0.7 cm^3. The samples were in a micro-container made of quartz inside the tube. The tube contained a diffusion source,[50] which was a pulverized mixture of 75% GaP and 25% Zn (by wt.). A source of 4.5 mg was used in each run. The diffusion temperature ranged from 900°C to 920°C, depending upon the composition of the alloys. The temperature of the sample was kept a few degrees hotter than that of the source. The diffusion time was from 30 min to 2 hrs. The samples were annealed 3-4 hrs to increase the concentration of the Zn-O exciton complex[51] responsible for the red light. After annealing, the samples were relapped to remove the diffused layer. Ohmic contacts were made by alloying for 5 ∿ 8 min at

400 ∿ 500°C in a hydrogen atmosphere. An In dot was used for the n-side and an In-Zn (5%) dot for the p-side. The diode thus fabricated was etched for a few seconds to reduce surface leakage and then mounted on a TO-5 header with the n-side down. Contact to the p-side dot was made by ultrasonic bonding with 1 mil Au wire. The diameter of the dot on the p-side was less than 0.2mm.

The spectral distribution of the electroluminescence of these diodes was obtained using pulsed currents and an S-1 response photomultiplier tube cooled with dry ice. The monochromator was a Heath EU-700 instrument (f/6.8). A Princeton Applied Research 124 amplifier was used in the synchronous detection. Measurements were made for temperatures in the range 77 ∿ 300°K. The pulsed current was usually run at 1 kHz, with a pulse width of 50μsec.

A. Spectra from GaP Diodes

1. Spectra from solution-grown GaP (#615G-2-1)

The emission spectra of this diode are shown in Fig. 12 for various temperatures in the range 77-300°K. The I-V characteristic is shown in Fig. 13. The starting material appears to have contained Si, S, O, and N as residual impurities. The carrier concentration of one sample of the same lot was 1.1×10^{17} cm^{-3} at room temperature and the resistivity was 0.57Ω-cm. The 1.95eV emission which was observed in the cathodoluminescent spectrum also appears in the electroluminescent spectrum at liquid nitrogen temperature. This emission can be interpreted[42,43] as the pair recombination radiation between Si-Si (or Si-S), as we did for cathodoluminescent spectrum. This recombination is dominant at low

temperatures 77-186°K. With increasing temperature the red peak due to the Zn-O exciton recombination appears, along with the quenching of the Si emission.

The A line is known as the decay of an exciton bound to nitrogen isoelectronically substituted for a phosphorous atom. The emission line 32 meV below the energy gap is identified as the phonon replica of the A line (A-TA). The temperature dependence of the forbidden energy gap in pure GaP is known.[52,53] The (A-TA) emission decreases with decreasing temperature. Beside these recombination lines, emission at energy 2.2eV is observed in both forward and reverse bias (Fig. 16) emission. According to the following equation

$$E_g - h\nu = (E_A + E_D) \qquad (7)$$

(E_A+E_D) is 134 meV. This emission may be considered as due to Zn-Si or Zn-S. Bound-to-free recombination was not observed.

2. Spectra from the vapor grown GaP (#31270-11)

This crystal was grown by chemical transport with iodine. The carrier concentration and resistivity of another sample of the lot was measured as 1.7×10^{17} cm^{-3} and 0.3Ω-cm at room temperature. The forward bias emission spectra from this diode are shown in Fig. 14 for temperatures 77 ∿ 300°K. I-V curves are presented in Fig. 15. The radiation due to Zn-O exciton appears as observed by others.[54] The Si-related emission does not appear, which means that the samples grown with iodine transport techniques are not contaminated with Si. The phonon replica of the A line is observed, as in the solution grown sample. The energies of these emission lines are 32 meV below the

energy gap. This emission is therefore identified as (A-TA) emission. Nitrogen must therefore be present in these GaP crystals as an unintentionally added impurity.

Emission due to donor-valence-band transitions is observed at lower temperatures; at room temperature this emission is not seen because of the thermally broadened (A-TA) emission. Using the well known relation

$$E_g - h\nu = E_D - kT \qquad (8)$$

E_D is obtained as 93 meV. Since the ionization energy of the Te donor is 89.5 meV,[55] the n-type dopant of the sample may be identified as Te, unintentionally added.

The pair band involving Zn and Te predominates at liquid nitrogen temperatures. This emission vanishes above 144°K. According to Eq. (7), (E_A+E_D) is calculated as 157 meV. With the ionization energy of Zn(= 64 meV) Eq. (7) gives a donor ionization energy E_D of 93 meV. The high energy transition involves the radiative capture of free holes to Te donors, and the (A-TA) line at high temperatures. The green luminescence properties of the GaP diodes (both solution grown and vapor grown) are generally similar to those reported elsewhere.[32,33,56]

The cathodoluminescent spectrum of one sample of lot 31270 showed an emission band at 1.62eV at 77°K, which might be related to iodine. Forward bias emission does not show recombination at that energy, but the reverse bias emission at liquid nitrogen temperature shows a band at 1.62eV together with the recombination band due to the Zn-O exciton complex (See Fig. 16).

B. Spectra From the Alloy Diodes

1. Alloy diodes of < 0.5% ZnSe (#625GZ-8-1, #625GZ-4-A-2)

The forward and reverse biased emission from the alloy diodes is shown in Figs. 17, 18 and 20 for temperatures between 77°K and 300°K. The I-V characteristics of one of these appears in Fig. 19. As we see from Figs. 17(a) and 17(b) two different spectra were observed from the same sample; 17(a) immediately after fabrication, and 17(b) two weeks later. The spectra of Fig. 17(b) do not show the recombination due to the Zn-O complex; the peak at 1.56 eV is at lower energy than the Zn-O peak in 17(a), which is at $\sim$1.8 eV . Even though these samples were grown from gallium solution, the ZnSe material contained in the alloys was grown by vapor transport with iodine. It is not clear whether the emission band is related to iodine or to an unknown impurity.

Si-related pair recombination, which was observed in the cathodoluminescence spectrum, is also observed at 77°K and 153°K (Figs. 17 and 18). This emission predominates at low temperatures. The spectra from another diode (#625GZ-4-A-2) in Fig. 20 shows the Si emission at liquid nitrogen temperature with another emission band at lower energy. Fig. 20(a) indicates that there are two dominant radiations at 164°K, probably the emission due to the Zn-O complex and the unknown recombination center. The radiation of the Zn-O complex is sometimes observed, but sometimes not.

2. Alloy diodes of ∿ 1% ZnSe (#927CT-4)

Fig. 21 shows the forward and reverse bias emission spectra for temperatures of 77-300°K. The emission due to Zn-O appears in both forward and reverse bias emission at liquid nitrogen temperature. With the increase of temperature the energy peak has shifted to lower energy (∿ 1.65eV at 300°K). The reverse bias emission shows the emission band at energy ∿ 1.64eV together with the radiation due to Zn-O. This may be considered as the same radiation observed in the GaP diode (#31270-11) and the cathodoluminescent spectrum of GaP. The emission (at 1.44eV) which appeared in the cathodoluminescence spectrum of this alloy, does not appear in the electroluminescent spectra.

3. Alloy diode of ∿ 5% ZnSe (#SG61-1)

Fig. 22 shows forward and reverse bias emission at room temperature. The forward bias emission does not have any peak for energies greater than 1.3eV. The I-V characteristic is given in Fig. 23.

As we see from the alloy diodes a striking difference between the GaP diodes and the alloy diodes is the fact that the luminescence near the band-gap present in the GaP diodes does not appear in the alloy diodes. This quenching of the near band-gap luminescence may be due to impurity banding Auger mechanism,[35] the effect of screening of ionized impurities, an unknown nonradiative process, or combinations of these processes. This near band gap luminescence includes the donor-acceptor recombination, the bound-to-valence band recombination, and the decay of excitons bound to nitrogen atoms. The external quantum efficiency was not measured. But the efficiency of the alloy diodes is reduced by a

factor of 100 ∿ 500 compared to that of the GaP diodes. With the increase of content of ZnSe the efficiency becomes lower. The crystal quality of the alloy diodes is also poorer, and the background doping is much higher.

C. Reverse Bias Emission

Since Newman[57] first reported breakdown radiation in Si junctions, breakdown radiation has also been reported for Ge, GaAs, SiC, and GaP. p-n junctions can be separated into two classes, those in which breakdown is by the avalanche mechanism and those in which breakdown is by Zener field emission. For GaP the avalanche breakdown has been reported.[58-60] The phenomenon can be interpreted as an impact ionization process which often takes place locally at imperfections. The field inhomogeneity caused by imperfections produces small spots of luminescence. Usually the avalanche breakdown is associated with a photon emission where the spectrum is usually broad. Baraff's theory[61] gives about $1.5E_g(\simeq 3.4eV)$ for the ionization energy of hot carriers in GaP.

The reverse bias emission of the GaP and alloy diodes was obtained for various temperatures 77-300°K. The microscopic investigation of the light emission associated with the avalanche breakdown shows the well known appearance of one or several light spots and the sample boundary light emission as a line. With increase of current the light intensity grows. Those are probably associated with gallium precipitates or dislocations. The breakdown voltages of the solution grown samples ranged from 8 ∿ 12 volts. The vapor grown samples do not show any apparant breakdown. This may be explained by the fact that the vapor grown samples were relatively free from crystal imperfections like the gallium

precipitates seen in the solution grown samples. The observations from the GaP and alloy diodes emission spectra may be divided into three groups: 1) The spectra are broad, show a maximum near 1.8 ∿ 2.1eV, and do not show structure, 2) The spectra have some structure observed in the forward bias emission spectra, and 3) The spectra have both characteristics mentioned above.

1. Spectra with structure

This kind of spectrum is observed for the GaP and the alloy diodes. Figs. 16(a) and 16(b) show the emission of diode #615G-2-1 (GaP) with different bias at room temperature. The observation of Fig. 16(b) shows that the emission is almost identical with the forward bias emission; (A-TA) emission appears and the red emission possibly due to Zn-O is present even though the red peak has shifted to high energy compared to the forward bias emission due to Zn-O. This indicates the bias dependent spectrum. The emission at liquid nitrogen temperatures (Fig. 16(c)) has Si associated recombination and Zn related pair recombination. These emissions are almost identical with those at forward bias.

Another diode (#31270-11) also shows structure at liquid nitrogen temperatures; Zn-O complex and the unknown emissions (possibly due to iodine) are superposed on the broad spectrum.

This phenomenon is observed in alloy diodes at liquid nitrogen temperature; #625GZ-4-A-2 of Fig. 20(c), #625GZ-8-1 of Fig. 18(d), and #927CT-4 of Fig. 21(d). The shape of these reverse bias emission spectra is almost the same as that of forward bias emission spectra. The

structures in the spectra include Si associated emission, Zn-O recombination, and the unknown emission, all of which were explained earlier for the forward bias emission. The only difference is the fact that the reverse bias emission has a long high energy tail beyond about 2.2eV. The alloy diodes show structure only at nitrogen temperature. Their spectra are all broad.

2. Broad spectra

The reverse bias broad emission spectra are presented in Figs. 16(a), 16(d), 20(d), and 18. There is no apparent difference between the GaP and alloys. The spectra have a broad maximum between 1.8 ∿ 2.0eV. The intensity drop after the maximum is present in all observed diodes. The drop about 2.2eV is sharper for the GaP diodes than the alloy diodes. This broader maximum and slow drop in the alloy samples may be due to the presence of the impurity band and tailing. Finally, above about 2.55eV the spectrum is gone. The tail of alloy diodes goes to higher energy values than the GaP (See Fig. 24). If this is due to eventual $\Gamma_{15} \rightarrow \Gamma_1$ absorption this might indicate somewhat different band parameters in the alloys.

The change of the emission spectra of the alloy diode (#625GZ-8-1) with temperature is shown in Fig. 20. There is no broad emission at nitrogen temperature. With the increase of temperature we observe the broad spectra, which show typical avalanche breakdown emission. The spectra are almost independent of temperature, which indicate that the broad emission is associated with free electrons.

The reverse bias emission can be classified clearly with the above explained information: 1) the broad emission related to the avalanche plasma and so to an electron temperature rather than to the lattice temperature, 2) the emission associated with recombination centers, which is related to lattice temperature.

There are two different types of explanations of the avalanche breakdown emission. Wolff[62] has explained the shape of the spectrum by assuming a combination of inter- and intraband transitions of hot carriers. This theory naturally gives a structure to the broad spectra. Figielski and Torun[63] proposed a bremsstrahlung theory. The radiation is from the bremsstrahlung of hot carriers in the Coulomb field of charged impurities. They assumed that the electron gas is Maxwellian. The spectrum of radiation is given by

$$I(h\nu) \simeq \exp\left(-\frac{h\nu}{k_B T_e}\right) \qquad (9)$$

where T_e is the electron gas temperature. Shewchun and Wei[64] improved the theory with a suitable high field electron distribution function.

Wolff's model cannot describe the spectra from our samples because the spectra due to the avalanche breakdown are broad without structure. Fig. 24 shows the curves of $\log I(h\nu)$ vs $h\nu$ for the GaP and alloy diodes at 300°K. At energies above 2.2eV the GaP diodes give good straight lines. The curves of the alloy diodes gradually bend over and show much shorter straight parts, compared to the GaP diode. Bremsstrahlung theory cannot explain the whole spectrum, but it is only good in the high energy range.

VI. Summary and Conclusion

GaP and $(GaP)_x(ZnSe)_{1-x}$ alloy crystals were grown by the solution method from gallium melt and the vapor transport technique using iodine as transport agent. Alloy composition attained during the grant period were up to 8% ZnSe in GaP. All crystals were n-type, even though most of the crystals were not doped intentionally.

The study of electronic transport measurements in the temperatures of 8 ∿ 360°K showed that the scattering in the alloys is quite different from that in GaP. The mobility is a monotonically increasing function of temperature at the temperatures observed. The ionized impurity scattering is dominant for temperatures above 150°K. The mobility can be explained as a combination of ionized impurity and acoustic phonon scattering. The mobility decreases strongly below 150°K, probably due to the presence of a hopping mechanism in an impurity band. The mobility decreases with increase of ZnSe content; the mobility of a 5% ZnSe alloy is 7 $cm^2/V \cdot sec$ at room temperature. Dipole scattering necessarily present in this alloy system is found to give a negligible contribution to scattering, up to the 5% level. The Hall coefficient shows the broad maximum in the transition region of the $\rho(T)$ curves, which indicates hopping conduction. The activation energy ε_3 related to the hopping mechanism is observed to be about 4 meV for temperatures below about 50°K.

Cathodoluminescent studies reveal unknown deep radiation centers in the GaP and the alloys. Donor-acceptor pair recombination between Zn and Se is not observed in the alloys. This indicates that the impurities influence the radiative recombination in the alloys.

A striking difference in the emission spectra between the Zn diffused GaP and the Zn-diffused alloy diodes is the fact that the near band gap emission present in GaP doesn't appear in the alloy diodes in the temperature range 77 ∿ 300°K. The near band gap emission includes the donor-acceptor pair recombination, the exciton emission bound to nitrogen atoms, and donor-valence band radiation recombination. At liquid nitrogen temperature, Si-related (as acceptor) donor-acceptor recombination for the solution grown samples and the Zn-O complex excitonic recombination for the vapor grown samples predominate in the alloy diodes. These emissions are quenched with increasing temperature. A new emission band related to an unknown impurity appears at room temperature. The alloy diode of 5% ZnSe doesn't show any emission peak for photon energies greater than 1.3 eV at room temperature.

The new emission band at the energy of 1.62 eV observed in the cathodoluminescence spectrum of the vapor grown GaP sample at liquid nitrogen temperature also appears in the reverse bias emission of the vapor grown GaP and alloy diodes. This could be due to iodine.

The reverse bias emission from the alloy diodes shows the broad spectra associated with avalanche breakdown except at liquid nitrogen temperature. The shape of the reverse bias spectra is almost the same as that at forward bias. The broad emission of alloy diodes is almost the same as that of the GaP diodes, but the alloy diodes have higher energy tails than the GaP diodes. This may be attributed to different band parameters. Further basic study of the near band-edge optical properties should elucidate the band structure in the alloys.

VII. Acknowledgments

The materials preparation and crystal characterization were performed in the Materials Preparation Laboratory at Brown University. Some analysis was performed at RCA Laboratories, Princeton, N. J. and we thank Drs. W. M. Yim and H. H. Whittaker for this. It is a pleasure to thank P. W. Yu for much of the measurement and analysis reported here, and R. Beaulieu and R. Kershaw for their contributions in crystal growth, analysis, and sample preparation.

References

1. N. A. Goryunova, The Chemistry of Diamond-like Semiconductors, Chapman and Hall, Ltd., London, 1965), p. 148.
2. W. M. Yim, J. Appl. Phys. **40**, 2617 (1969)
3. W. M. Yim, J. P. Dismukes and H. Kressel, RCA Rev. 31, 662 (1970).
4. S. M. Ku and L. J. Bodi, J. Phys. Chem. Solids 29, 2077 (1968).
5. I. Bertoti, M. Forkas-Jahnke, M. Horsey, T. Nemath and K. Richter, Proceedings of International Conference on Luminescence (Hungarian Academy of Sciences and the Eotvos Lorand Physical Society, Budapest, 1966). p. 235; I. Bertoti, E. Barta, J. Schanda, and P. Suiszt, ibid., p. 241.
6. See, for instance, P. J. Dean in Applied Solid State Science, Vol. 1, p. 2, (Academic Press, New York, 1969).
7. M. Glicksman, D. Gutman and W. M. Yim, Appl. Phys. Lett. 16, 366 (1970).
8. H. Scafer, Chemical Transport Reaction (Academic Press, Inc., New York, 1964).
9. See, for instance, J. W. Faust, Jr. and H. F. John, J. Phys. Chem. Solids 25, 1407 (1964).
10. A. V. Voitsekhovski and V. P. Drobyazko, and V. K. Mityorev, Soviet Physics J. #1, 159 (1969).
11. A. D. Stuckes and R. P. Chasman, J. Phys. Chem. Solids 25, 469 (1964).
12. H. Fritzsche, Phys. Rev. 89, 406 (1955).
13. N. F. Mott and W. D. Morse, Advan. Phys. 10, 107 (1961).
14. A. Miller and E. Abrahams, Phys. Rev. 120, 745 (1960).

15. H. C. Casey, Jr., F. Ermanis, and K. B. Wolfstirm, J. Appl. Phys. 40, 2945 (1969).

16. M. Toyama, M. Naito, and A. Kasami, Jap. J. Appl. Phys. 8, 358 (1969).

17. S. A. Abagyan, V. I. Amosov, A. P. Izergin, and R. S. Krupyshev, Sov. Phys.-Sem. 4, 1282 (1971).

18. H. Brooks, in Advances in Electronics and Electron Physics, ed. L. Marton (Academic Press, New York, 1955) vol. VII,, p. 87.

19. R. B. Dingle, Phil. Mag. 46, 831 (1955).

20. A. S. Barker, Phys. Rev. 165, 917 (1968).

21. A. Kasami, J. Phys. Soc. Japan 24, 551 (1968).

22. J. Bardeen and W. Shockley, Phys. Rev 80, 72 (1950).

23. R. Stratton, J. Phys. Chem. Solids 23, 1011 (1962).

24. A. D. Boardman, Proc. Phys. Soc. 85, 141 (1965).

25. E. Haga and H. Kimura, J. Phys. Soc. Japan 19, 658 (1964).

26. M. Glicksman, Phys. Rev. 111, 125 (1958).

27. J. J. Tietjen and L. R. Weisberg, Appl. Phys. Lett. 7, 261 (1965).

28. D. G. Thomas, M. Gershenzon, and F. A. Trumbore, Phys. Rev. 133, A269 (1964).

29. D. G. Thomas and J. J. Hopfield, Phys. Rev. 150, 680 (1966).

30. C. H. Henry, P. J. Dean, and J. D. Cuthbert, Phys. Rev. 166, 754 (1968).

31. T. N. Morgan, B. Welber, and R. N. Bhargava, Phys. Rev. 166, 751 (1968).

32. M. R. Lorenz, T. N. Morgan, M. H. Pilkuhn, and G. P. Pettit, J. Phys. Soc. Japan 21, 283 (1966).

33. P. J. Dean, M. Gershenzon, and G. Kaminsky, J. Appl. Phys. 38, 5332 (1967).

34. R. N. Bhargava, Phys. Rev. B2, 387 (1970).

35. P. J. Dean and C. H. Henry, Phys. Rev. 176, 928 (1968).

36. A. Addamiano, J. Electrochem. Soc. 107, 1006 (1960).

37. J. C. Tsang, P. J. Dean, and P. T. Landsberg, Phys. Rev. 173, 814 (1968).

38. M. Gershenzon, F. A. Trumbore, R. M. Mikulyak, and M. Kowalchik, J. Appl. Phys. 36, 1528 (1965); 37, 483 (1966).

39. J. D. Cuthbert, C. H. Henry, and P. J. Dean, Phys. Rev. 170, 739 (1968).

40. A. N. Pikhtin and D. A. Yas'kov, Soviet Phys.-Solid State 11, 1787 (1860).

41. K. P. Sinha and M. diDomenico, Jr., Phys. Rev. B1, 2623 (1970).

42. P. J. Dean, C. J. Frosch, and C. H. Henry, J. Appl. Phys. 39, 5631 (1968).

43. M. R. Lorenz and M. H. Pilkuhn, J. Appl Phys. 38, 61 (1967).

44. R. N. Bhargava, Bull. Am. Phys. Soc. Series II, 16, No. 3, 409 (1971).

45. M. Lizets and G. K. Knoluyanov, Sov. Phys.-Solid State 8, 463 (1966).

46. N. P. Bogoroditskii, A. N. Pikhtin, and D. A. Yas'kov, Sov. Phys-Solid State 9, 2297 (1968).

47. W. H. Hackett, Jr., R. H. Saul, H. W. Verleur, and S. J. Bass, Appl. Phys. Lett. 16, 477 (1970).

48. R. A. Logan, H. G. White and W. Wiegmann, Solid State Electronics 14, 55 (1971).

49. R. J. Robinson and Z. K. Kun, Appl. Phys. Lett. 15, 371 (1969).

50. M. Gershenzon, R. A. Logan, and D. F. Nelson, Phys. Rev. 149, 580 (1966).

51. A. Onton and M. R. Lorenz, Appl. Phys. Lett. 12, 115 (1968).

52. M. R. Lorenz, G. D. Pettit, and R. C. Taylor, Phys. Rev. 171, 876 (1968).

53. M. B. Panish and H. C. Casey, Jr., J. Appl. Phys. 40, 163 (1969).

54. See, for example, M. R. Lorenz and M. Pilkuhn, J. Appl. Phys. 37, 4094 (1966).

55. P. J. Dean, R. A. Faulkner, and S. Kimura, Phys. Rev. B2, 4062 (1970).

56. E. G. Diershke and G. L. Pearson, J. Appl. Phys. 41, 321 (1970).

57. R. Newman, Phys. Rev. 100, 700 (1955).

58. M. Gershenzon and R. M. Mikulyak, J. Appl. Phys. 32, 1338 (1961).

59. R. A. Logan and A. G. Chynoweth, J. Appl. Phys. 33, 1649 (1962).

60. M. H. Pilkuhn, J. Appl. Phys. 40, 3162 (1969).

61. G. A. Baraff, Phys. Rev. 128, 2507 (1962).

62. P. A. Wolff, J. Phys. Chem. Solids 16, 184 (1960).

63. T. Figielski and A. Torun, Int. Conf. Phys. Semiconductors, Exeter, (1962), p. 863.

64. J. Shewchun and L. Y. Wei, Solid-State Electron. 8, 485 (1965).

MG,PWY/geg,sw

Figure Captions

Fig. 1. Resistivity ρ vs the inverse of temperature $10^3/T$ of the alloys.

Fig. 2. Resistivity ρ vs the inverse of temperature $10^3/T$ of the samples of lot 625GZ and SG77.

Fig. 3. Resistivity ρ and Hall coefficient R_H vs the inverse of temperature $10^3/T$ of the samples of lot 625GZ and SG77.

Fig. 4. Resistivity ρ and Hall coefficient R_H vs the inverse of temperature $10^3/T$ of the samples of lot 1110SG.

Fig. 5. Resistivity ρ and Hall coefficient R_H vs the inverse of temperature $10^3/T$ of sample #927CT-7.

Fig. 6. Resistivity ρ and Hall coefficient R_H vs the inverse of temperature $10^3/T$ of sample #SG61-2.

Fig. 7. Hall mobility μ_H vs temperature T of the alloys and GaP.

Fig. 8. Comparison of the calculated ionized impurity scattering and dipole scattering with the experimental Hall mobility of sample #625GZ-1. The dipole density 7.1×10^{19} cm^{-3} and $9.7 \times 10^{-19} cm^{-3}$ are the numbers for 0.4 and 0.5% ZnSe, with the calculated ionized impurity density $N_I = 5.4 \times 10^{19} cm^{-3}$.

Fig. 9. Hall mobility μ_H vs the inverse of temperature of the alloys.

Fig. 10. Hall mobility μ_H vs the inverse of temperature of the samples of lot 625GZ and SG77.

Fig. 11. Cathodoluminescent spectra of the GaP and alloys at liquid nitrogen temperature.

Fig. 12. The forward bias emission of the solution grown GaP diode (#615G-2-1).

Fig. 13 The I-V characteristics of the GaP diode (#615G-2-1) at 300°K and 77°K.

Fig. 14. The forward bias emission of the vapor transport GaP diode (#31270-11).

Fig. 15. The I-V characteristics of the GaP diode (#31270-11) at 300°K and 77°K.

Fig. 16 The reverse bias emission of the GaP diodes(#615G-2-1 and #31270-11). Fig. (a) and (b) show the different spectra from the same diode at room temperature. The difference of spectra comes from the difference of bias applied. Fig. (b) is observed with higher bias than Fig. (a).

Fig. 17. The forward bias emission of the alloy diode (#625GZ-8-1). The spectrum of (a) was observed immediately after the fabrication. (b) was observed two weeks later.

Fig. 18. The reverse bias emission of the alloy diode (#625GZ-8-1).

Fig. 19. The I-V characteristics of the alloy diodes (#625GZ-8-1) at 300°K and 77°K.

Fig. 20. The forward and reverse bias emission of the alloy diode (#625GZ-4-A-2).

Fig. 21. The forward and reverse bias emission of the alloy diode (#927CT-4).

Fig. 22. The forward and reverse bias emission of the alloy diode (#SG61-1)at room temperature.

Fig. 23. The I-V characteristics of the alloy diode (#SG61-1) at room temperature.

Fig. 24. LogI($h\nu$) of the reverse bias emission of the GaP and alloy diodes vs $h\nu$ at 300°K.

List of Tables

Table I

Some properties of GaP and alloys with ZnSe

Number of the lot of sample	Sample	Method Growth	Doped Impurity	Type
615G	GaP	SG	ND	n
31270	GaP	VT	ND	n
1110SG	< 0.5% ZnSe*	SG	ND	n
625GZ	< 0.5% ZnSe*	SG	ND	n
SG77	< 0.5% ZnSe*	SG	S	n
927CT	∿ 1% ZnSe	VT	ND	n
SG61	∿ 5% ZnSe	SG	Cu	n
B430CT	∿ 8% ZnSe	VT	ND	-

SG: Solution grown

VT: Vapor transport

ND: Not intentionally doped

*: Some variation in results of Zn analysis for several samples

Table II

Activation energies in resistivity and mobility

Number of lot	Sample Number	Resistivity ε_3(meV)	Mobility E_A(meV)	"ε_1"
625GZ	625GZ-1	4.2	15	27
	625GZ-2	4.2	15	27
SG77	SG77-1	---	15	26
	SG77-2	4.1	15	26
	SG77-3	4.4	15	27
1110SG	1110SG-1	4.2	16	39
	1110SG-2	4.2	16	36
927CT	927CT-7	4.3	13	32
SG61	SG61-2	---	23	60

Table III

Cathodoluminescent Measurements for the GaP and Alloys at Liquid Nitrogen Temperature

Sample Number	Sample	Doped Impurity	1st Peak		Half width	2nd Peak	
615G-4	GaP	N.D.	6350 Å	1.95 eV	725 Å	12300 Å	1.01 eV
31270-100	GaP	N.D.	7650 Å	1.62 eV	1300 Å	11300 Å	1.10 eV
625GZ-10	<0.5% ZnSe	N.D.	6450 Å	1.92 eV	800 Å	14300 Å	0.87 eV
SG77-5	<0.5% ZnSe	S	5800 Å	2.14 eV	1100 Å		
927CT-6	∿1% ZnSe	N.D.	8600 Å	1.44 eV	2550 Å		
SG61-2	∿5% ZnSe	Cu	6500 Å	1.91 eV	1200 Å		
B430CT-1	8% ZnSe	N.D.	∿15600 Å	0.80 eV			

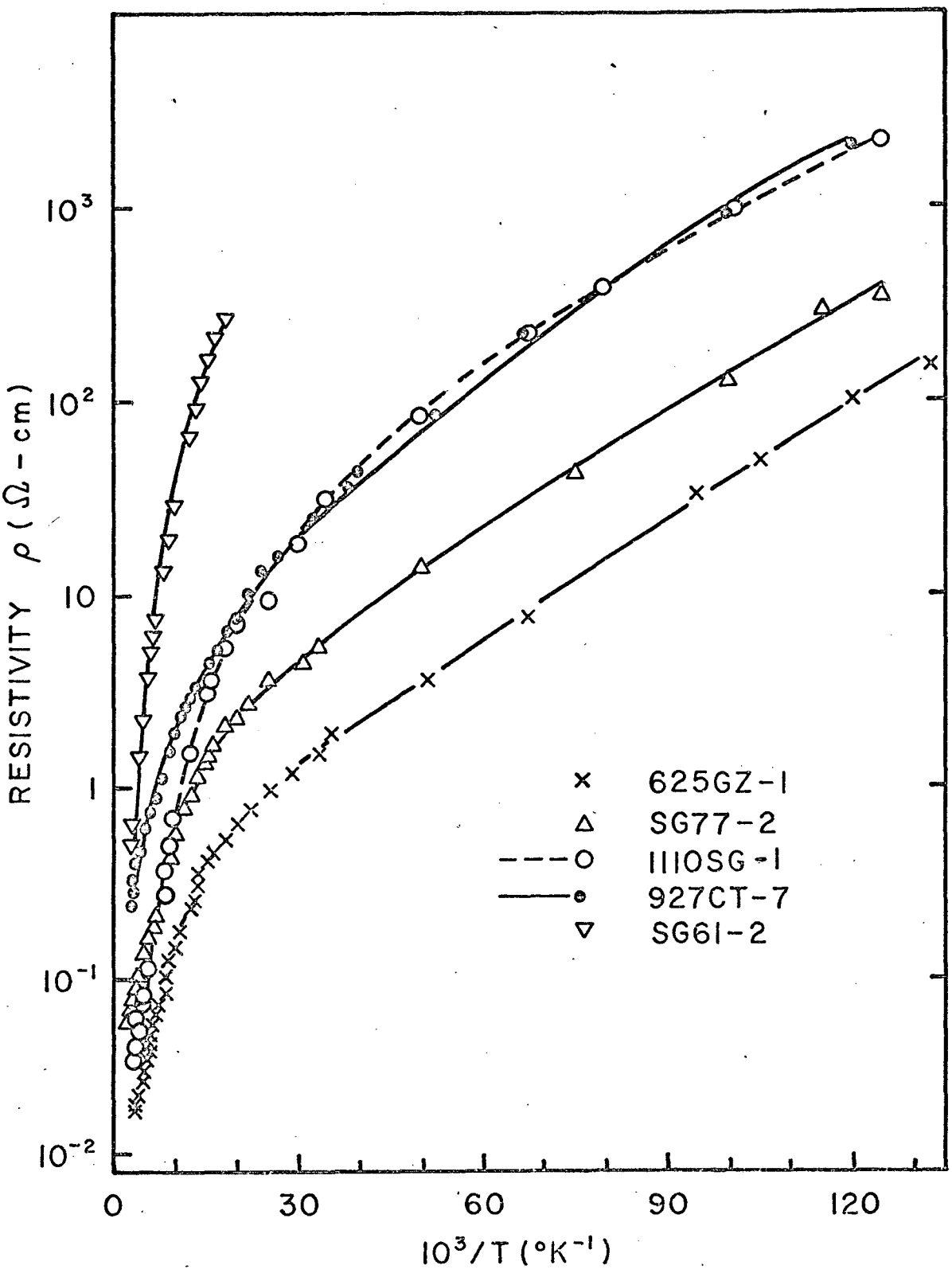
RESISTIVITY ρ (Ω - cm)
10³
10²
10
1
10⁻¹
10⁻²
0
30
60
90
120
10³/T (°K⁻¹)
625GZ-1
SG77-2
1110SG-1
927CT-7
SG61-2

FIGURE 1

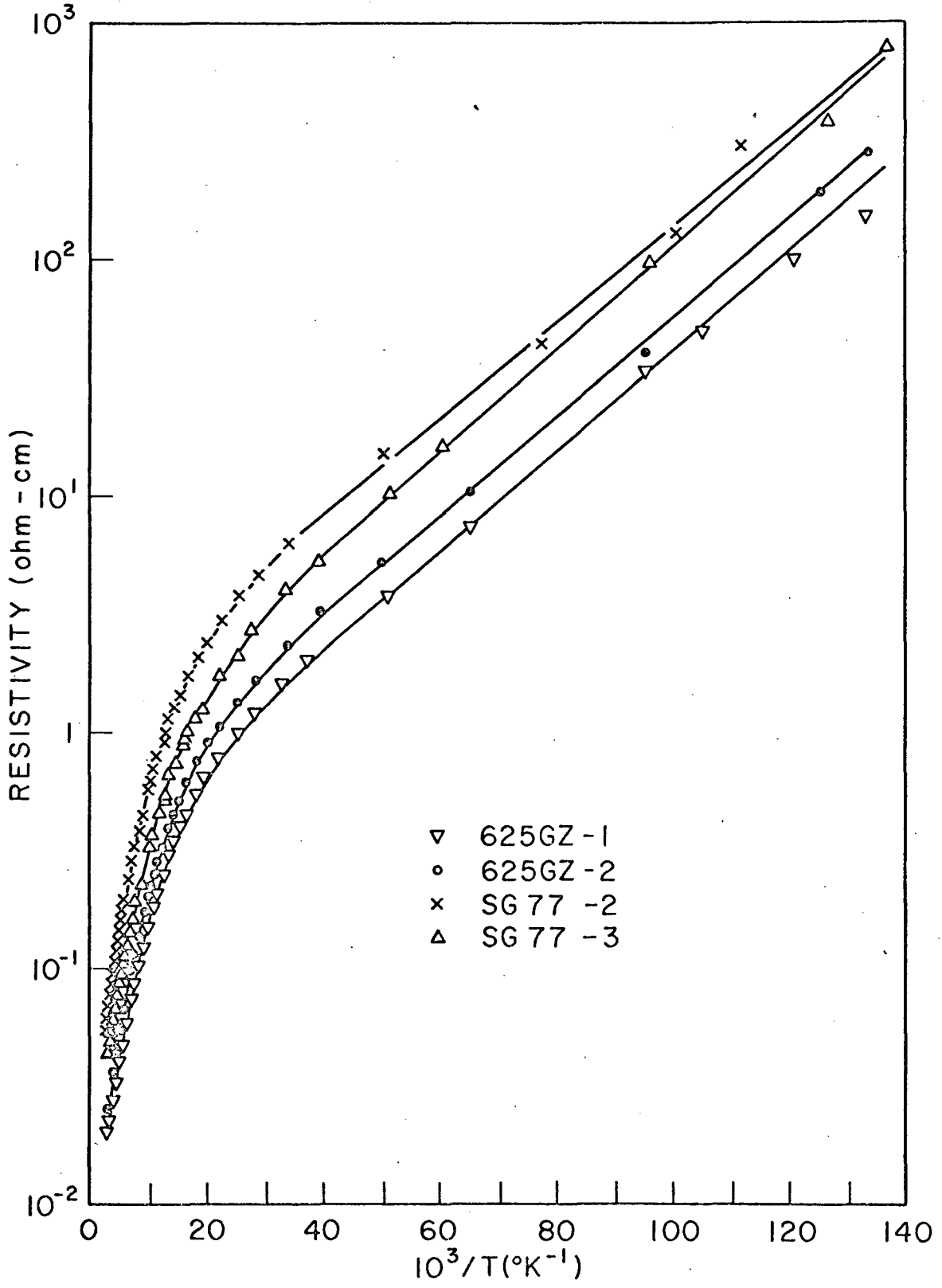
RESISTIVITY (ohm - cm)
10^3
10^2
10^1
1
10^{-1}
10^{-2}
0
20
40
60
80
100
120
140
$10^3/T(°K^{-1})$
625GZ-1
625GZ-2
SG 77 -2
SG 77 -3

FIGURE 2

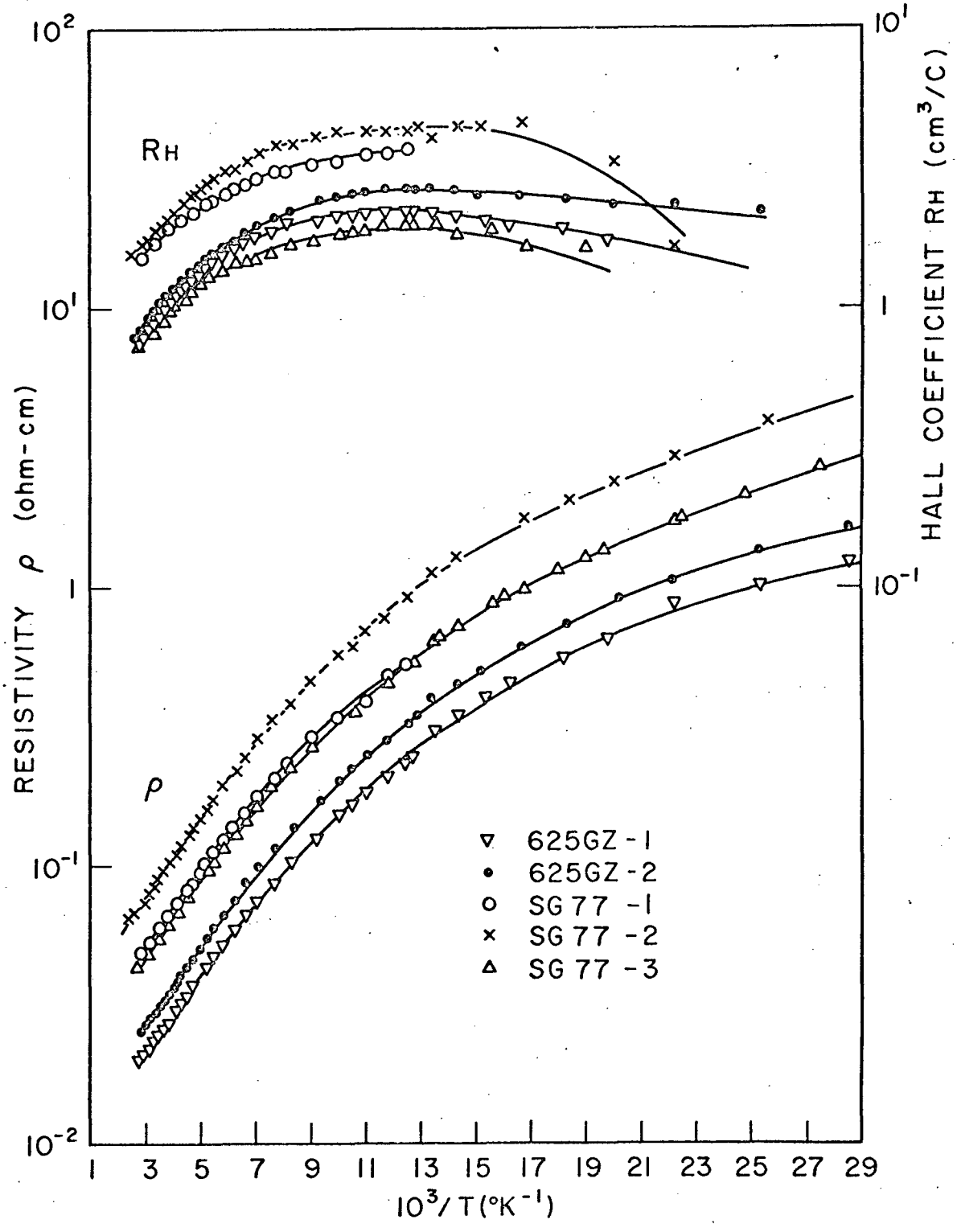
RESISTIVITY ρ (ohm-cm)
HALL COEFFICIENT RH (cm³/C)
10²
10¹
1
10⁻¹
10⁻²
RH
ρ
625GZ-1
625GZ-2
SG 77 -1
SG 77 -2
SG 77 -3
1 3 5 7 9 11 13 15 17 19 21 23 25 27 29
10³/T(°K⁻¹)

FIGURE 3

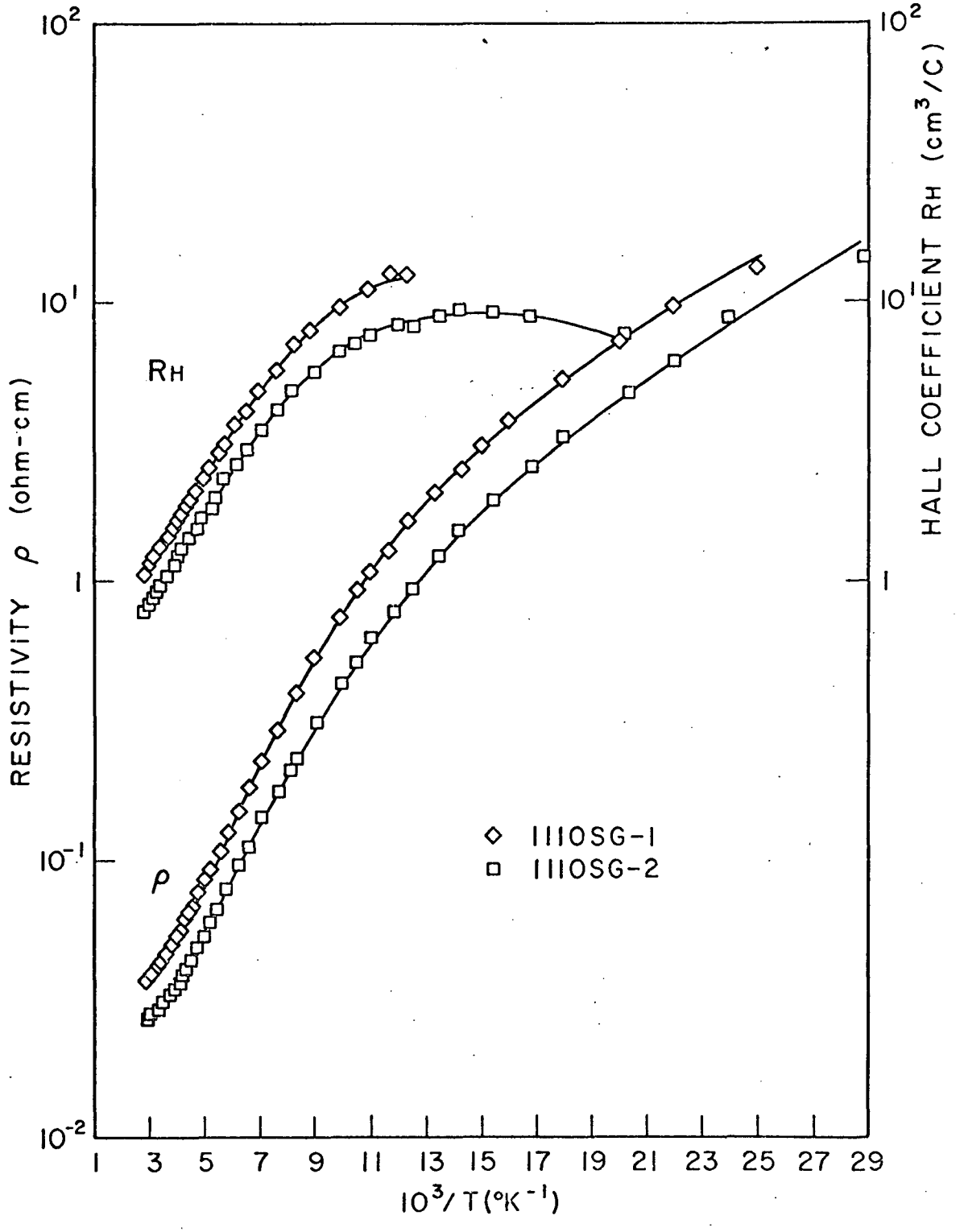
10^2
10^1
1
10^{-1}
10^{-2}
RESISTIVITY ρ (ohm-cm)
HALL COEFFICIENT RH (cm³/C)
RH
ρ
◇ 1110SG-1
□ 1110SG-2
1 3 5 7 9 11 13 15 17 19 21 23 25 27 29
10³/T(°K⁻¹)

FIGURE 4

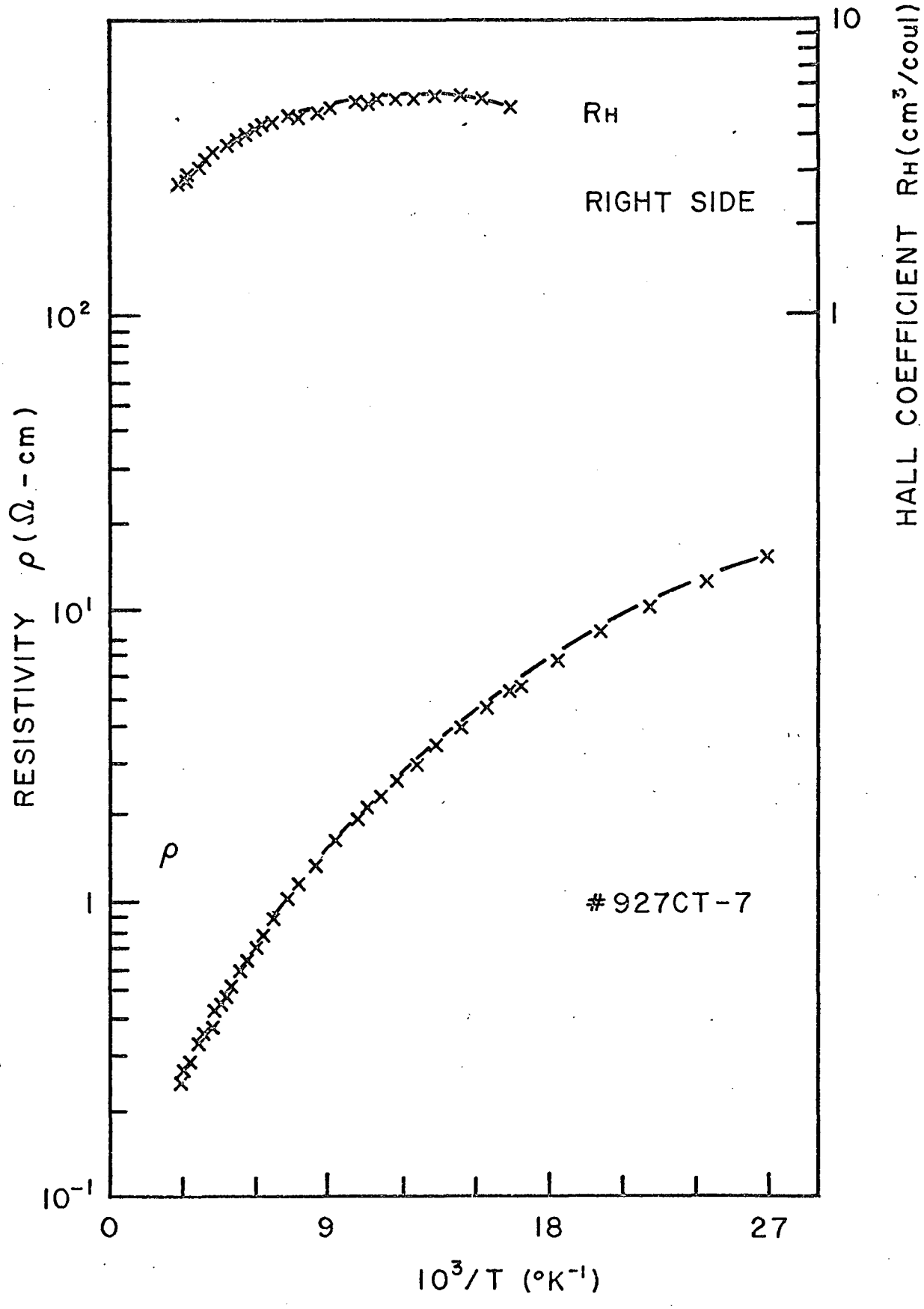
RH
RIGHT SIDE
ρ
#927CT-7
RESISTIVITY ρ (Ω - cm)
HALL COEFFICIENT RH (cm³/coul)
10²
10¹
1
10⁻¹
10
1
0
9
18
27
10³/T (°K⁻¹)

FIGURE 5

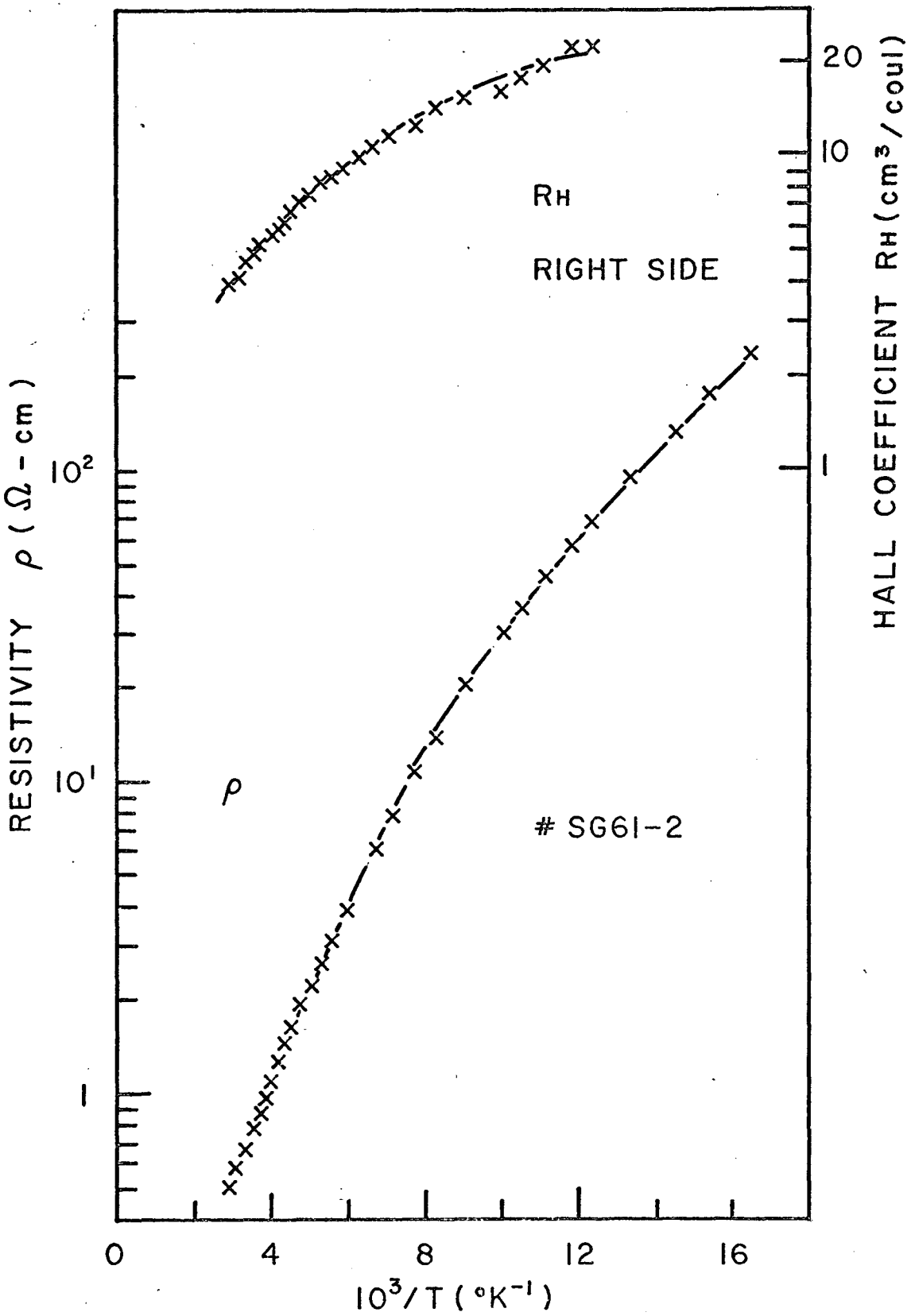
RESISTIVITY ρ (Ω - cm)
HALL COEFFICIENT RH (cm³/coul)
RH
RIGHT SIDE
ρ
SG61-2
10²
10¹
1
20
10
1
0
4
8
12
16
10³/T (°K⁻¹)

FIGURE 6

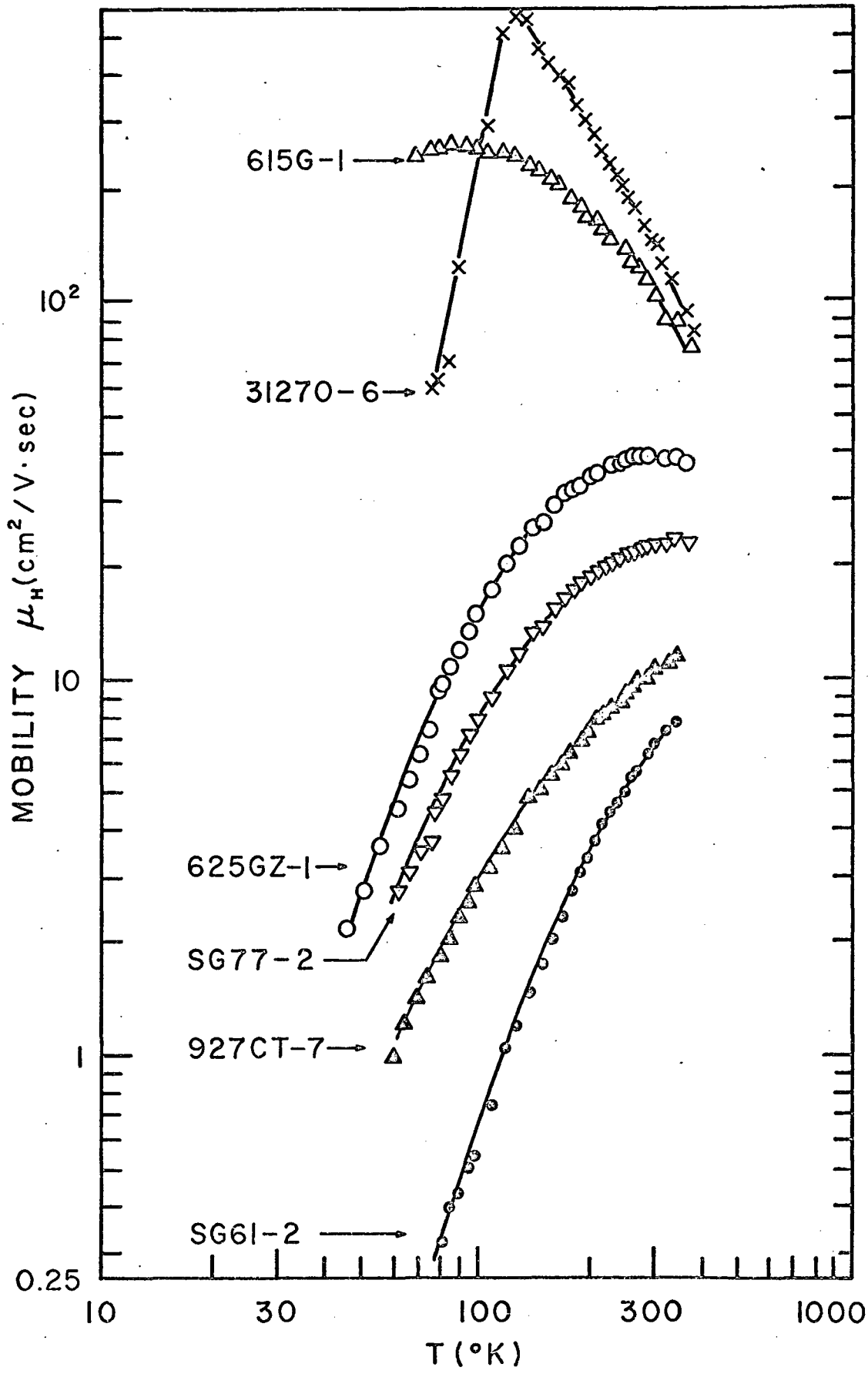
615G-1
31270-6
625GZ-1
SG77-2
927CT-7
SG61-2
MOBILITY μ_H(cm²/V·sec)
10²
10
1
0.25
10
30
100
300
1000
T(°K)

FIGURE 7

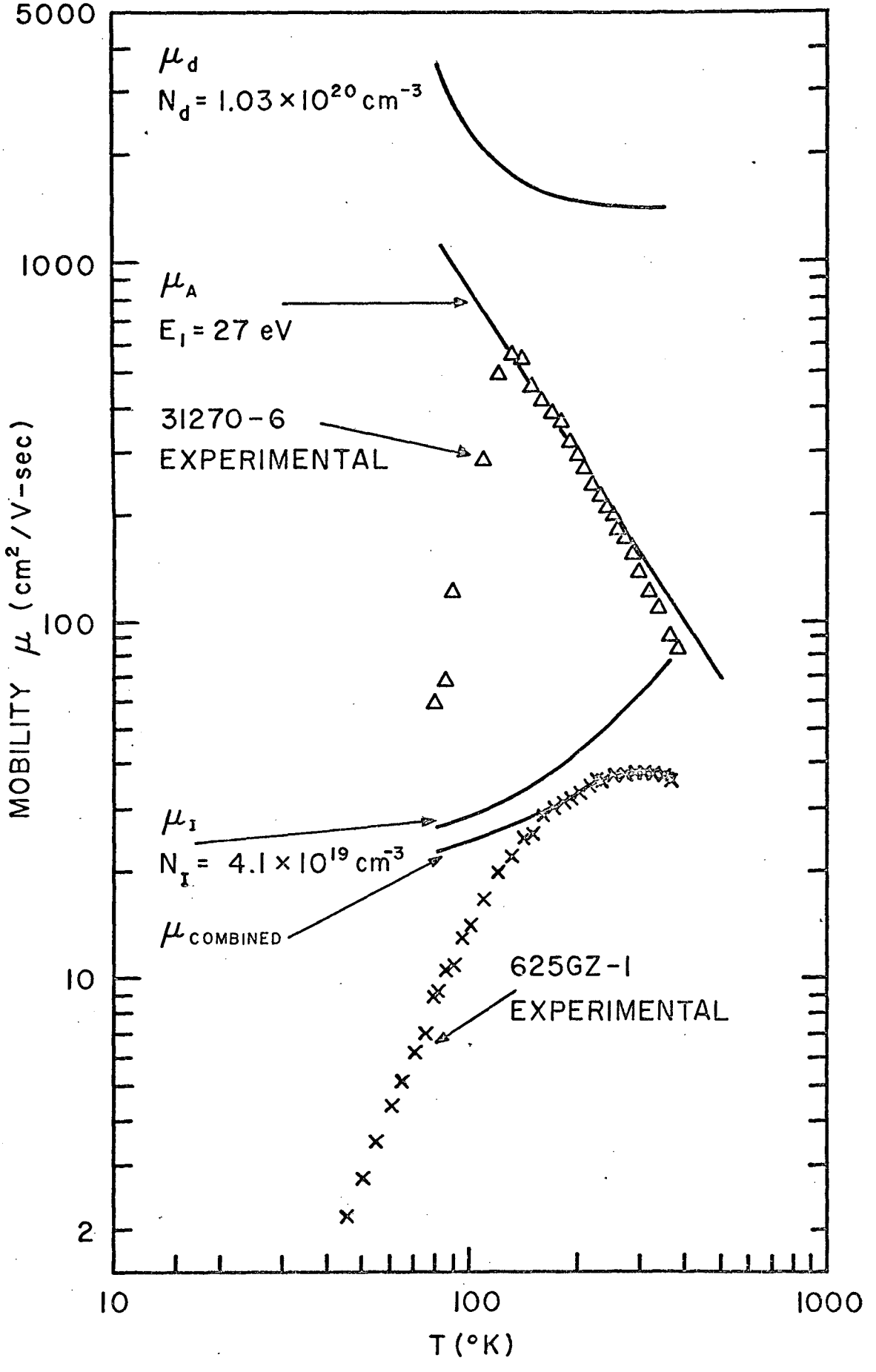
5000
1000
100
10
2
MOBILITY μ (cm²/V-sec)
μd
Nd = 1.03×10²⁰ cm⁻³
μA
EI = 27 eV
31270-6
EXPERIMENTAL
μI
NI = 4.1×10¹⁹ cm⁻³
μCOMBINED
625GZ-1
EXPERIMENTAL
10
100
1000
T (°K)

FIGURE 8

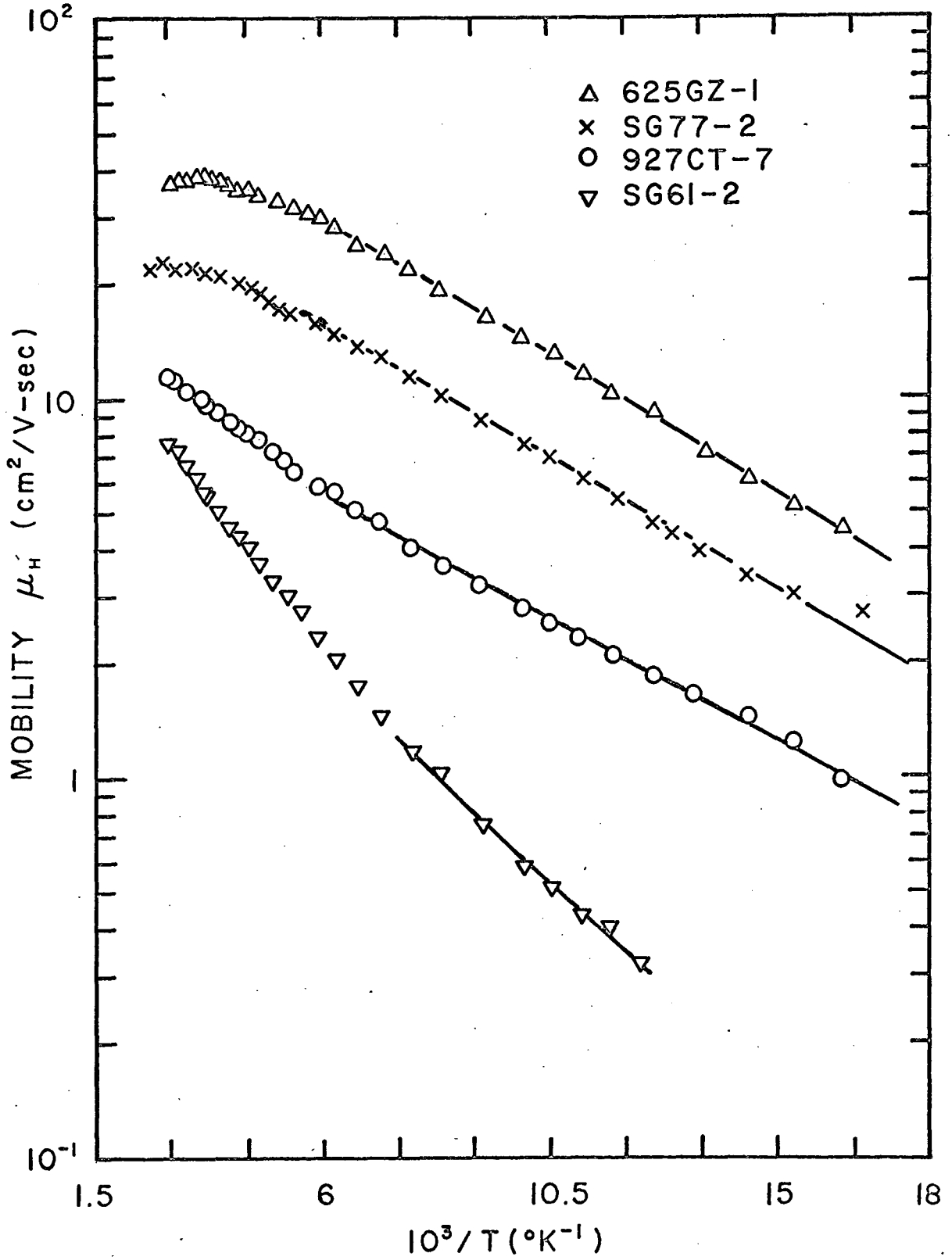
10^2
10
1
10^{-1}
MOBILITY μ_H (cm^2/V-sec)
△ 625GZ-1
× SG77-2
○ 927CT-7
▽ SG61-2
1.5
6
10.5
15
18
$10^3/T$ ($°K^{-1}$)

FIGURE 9

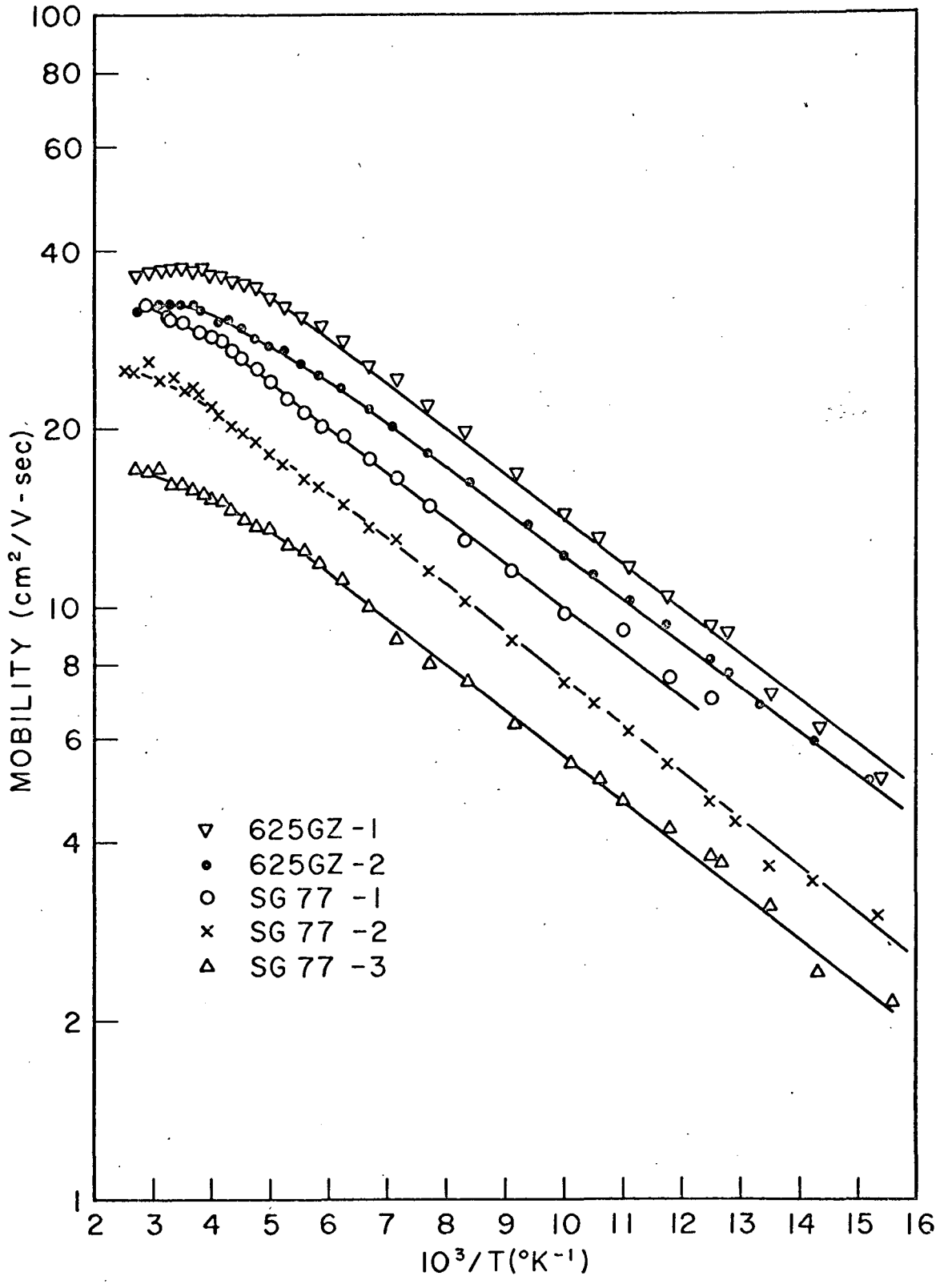
100
80
60
40
20
10
8
6
4
2
1
MOBILITY (cm²/V-sec)
2
3
4
5
6
7
8
9
10
11
12
13
14
15
16
10³/T(°K⁻¹)
625GZ-1
625GZ-2
SG 77 -1
SG 77 -2
SG 77 -3

FIGURE 10

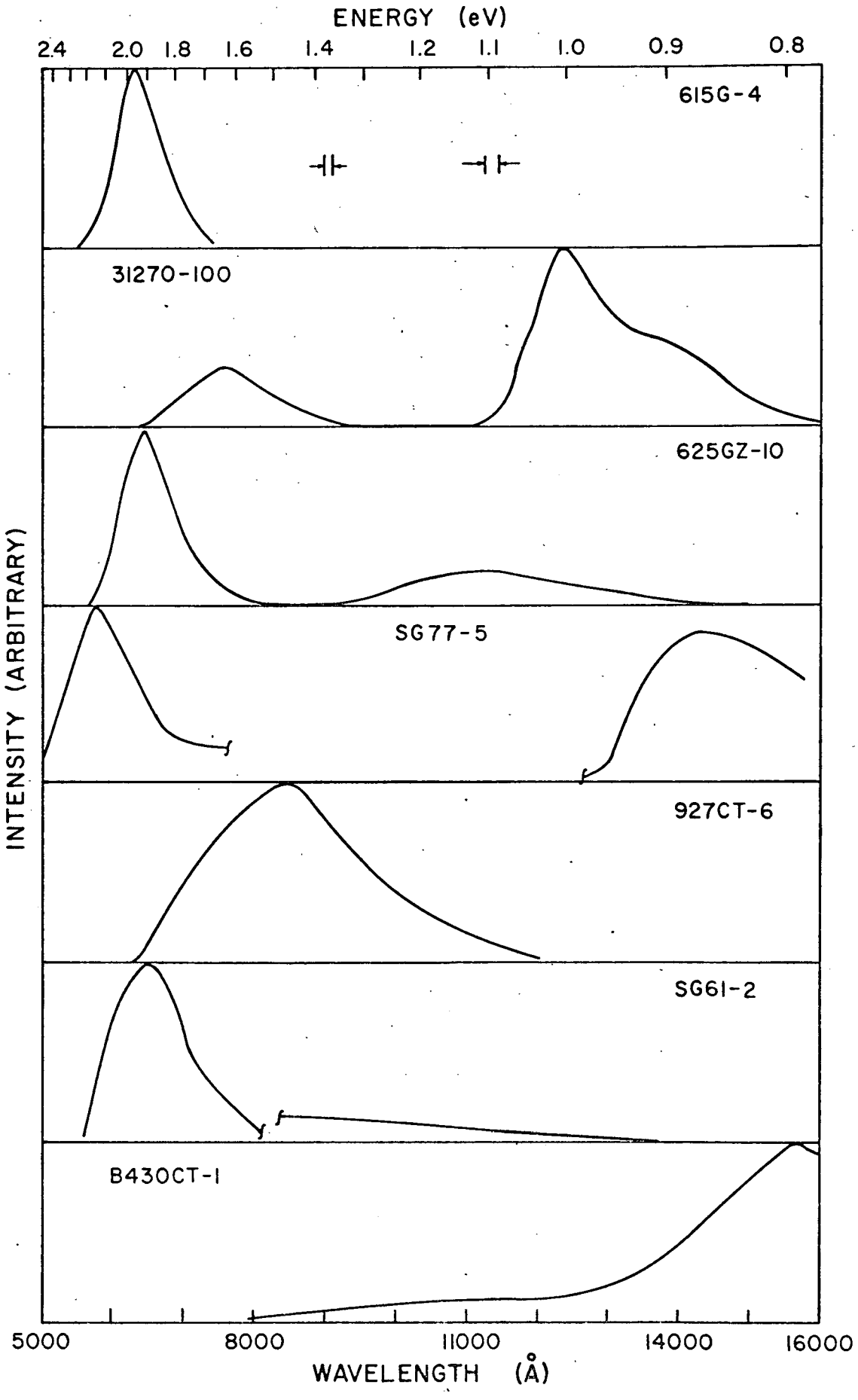
ENERGY (eV)
2.4
2.0
1.8
1.6
1.4
1.2
1.1
1.0
0.9
0.8
615G-4
31270-100
625GZ-10
SG77-5
927CT-6
SG61-2
B430CT-1
INTENSITY (ARBITRARY)
5000
8000
11000
14000
16000
WAVELENGTH (Å)

FIGURE 11

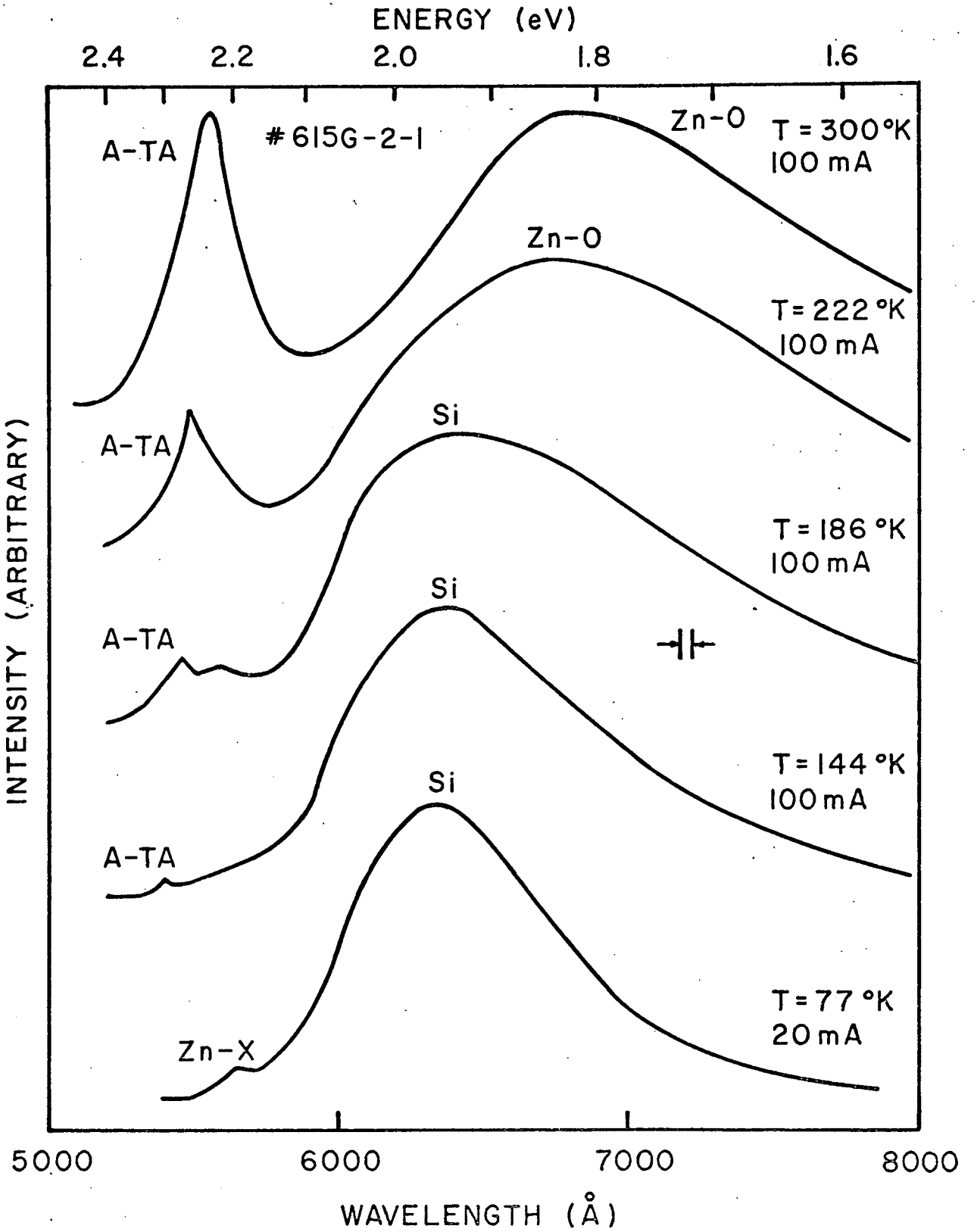
ENERGY (eV)
2.4
2.2
2.0
1.8
1.6
#615G-2-1
A-TA
Zn-O
T = 300°K
100 mA
Zn-O
T = 222 °K
100 mA
A-TA
Si
T = 186 °K
100 mA
A-TA
Si
T = 144 °K
100 mA
A-TA
Si
T = 77 °K
20 mA
Zn-X
INTENSITY (ARBITRARY)
5000
6000
7000
8000
WAVELENGTH (Å)

FIGURE 12

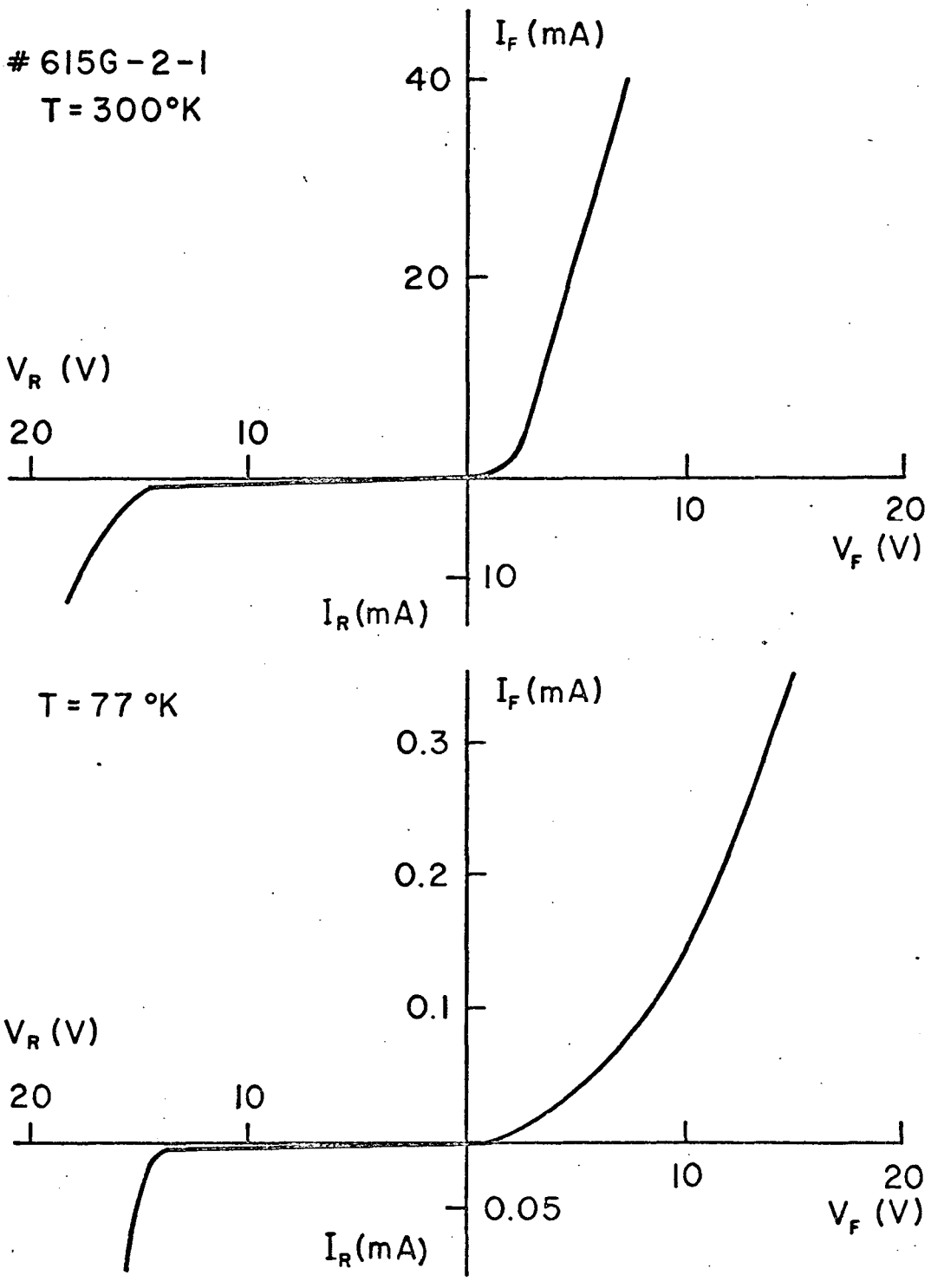
#615G-2-1
T = 300°K
I_F (mA)
40
20
V_R (V)
20
10
10
20
V_F (V)
10
I_R (mA)
T = 77 °K
I_F (mA)
0.3
0.2
0.1
V_R (V)
20
10
10
20
V_F (V)
0.05
I_R (mA)

FIGURE 13

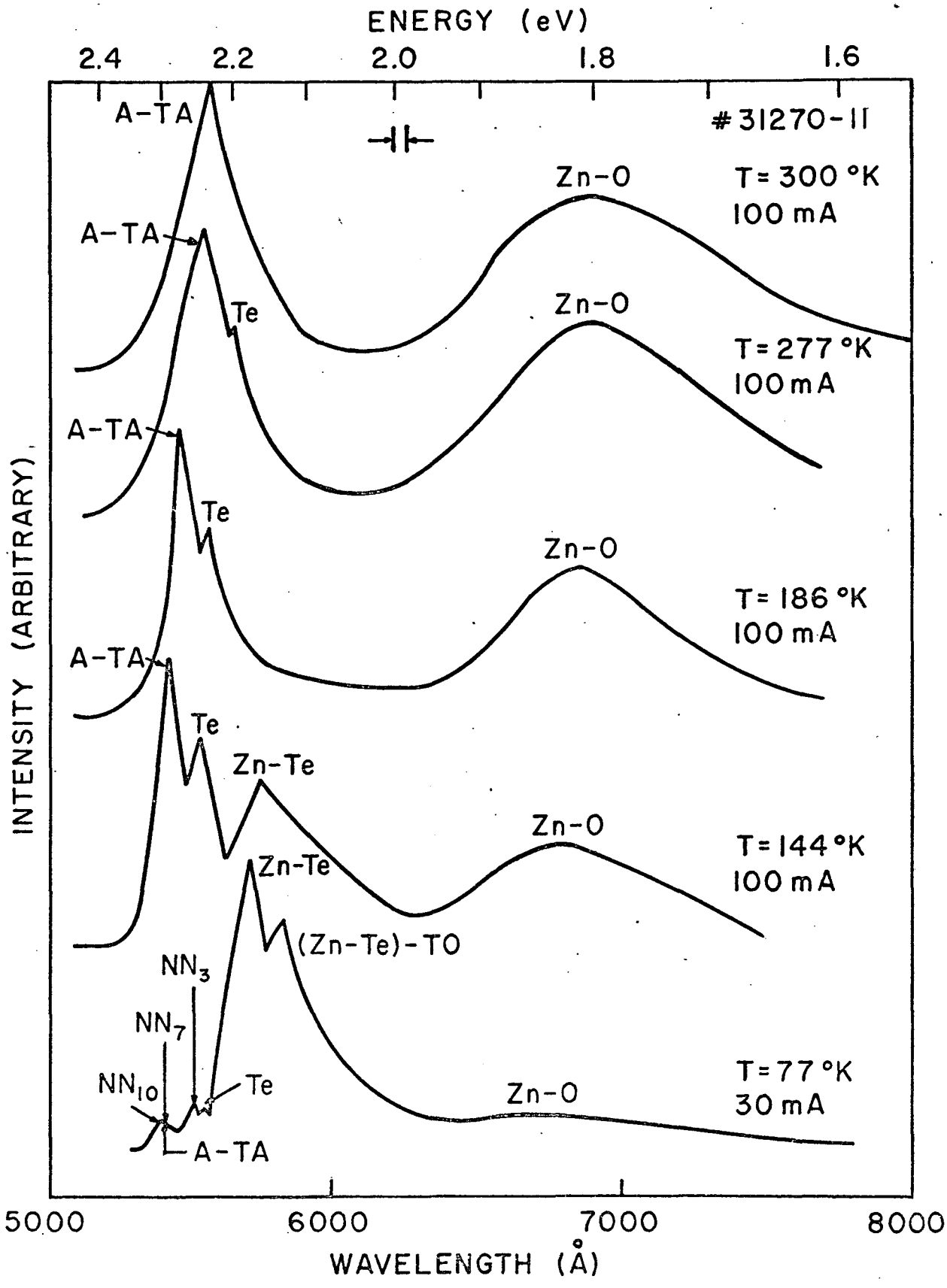
ENERGY (eV)
2.4
2.2
2.0
1.8
1.6
#31270-11
A-TA
Zn-O
T = 300 °K
100 mA
A-TA
Te
Zn-O
T = 277 °K
100 mA
A-TA
Te
Zn-O
T = 186 °K
100 mA
A-TA
Te
Zn-Te
Zn-O
T = 144 °K
100 mA
Zn-Te
(Zn-Te)-TO
NN3
NN7
NN10
Te
A-TA
Zn-O
T = 77 °K
30 mA
INTENSITY (ARBITRARY)
5000
6000
7000
8000
WAVELENGTH (Å)

FIGURE 14

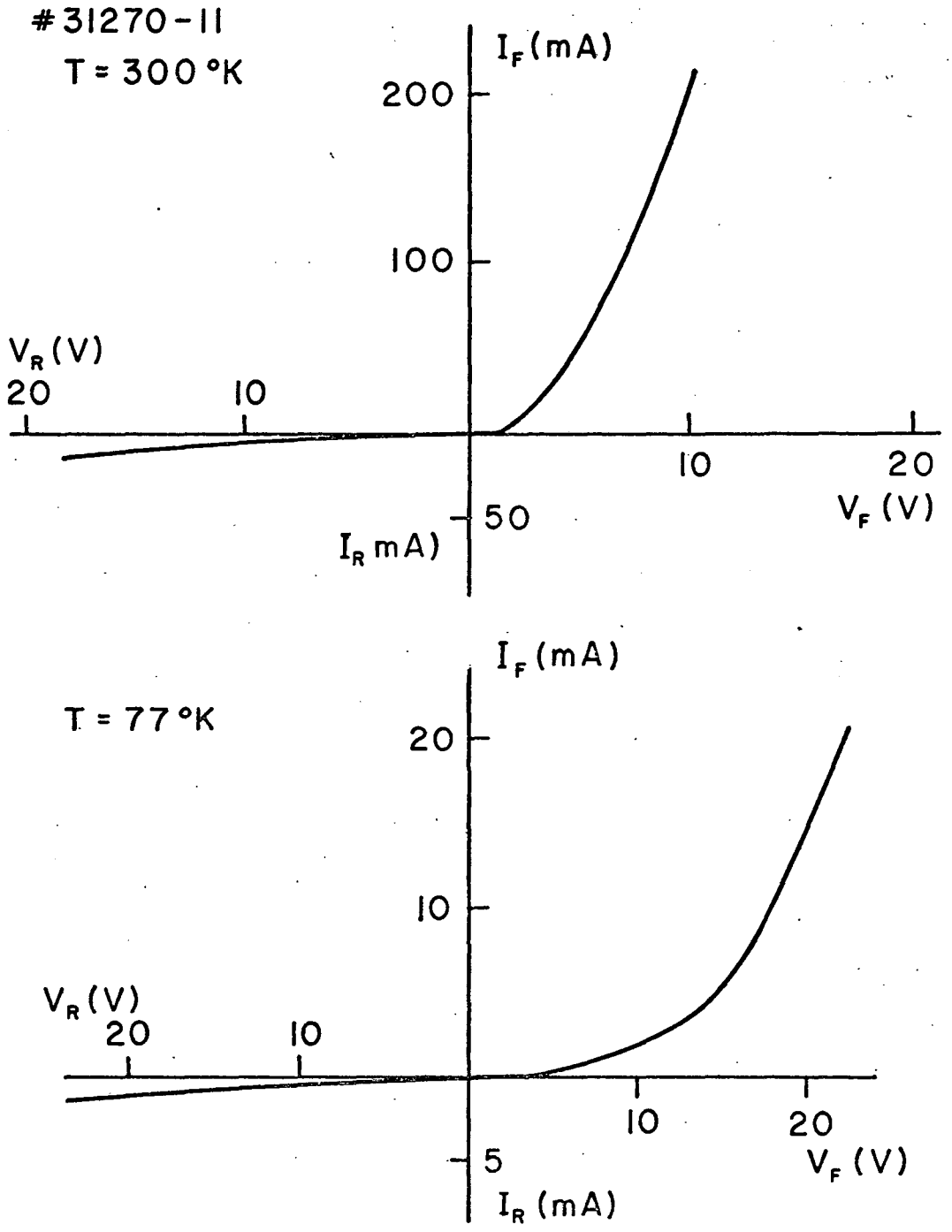
#31270-11
T = 300 °K
I_F (mA)
200
100
V_R (V)
20
10
10
20
V_F (V)
50
I_R mA)
I_F (mA)
T = 77 °K
20
10
V_R (V)
20
10
10
20
V_F (V)
5
I_R (mA)

FIGURE 15

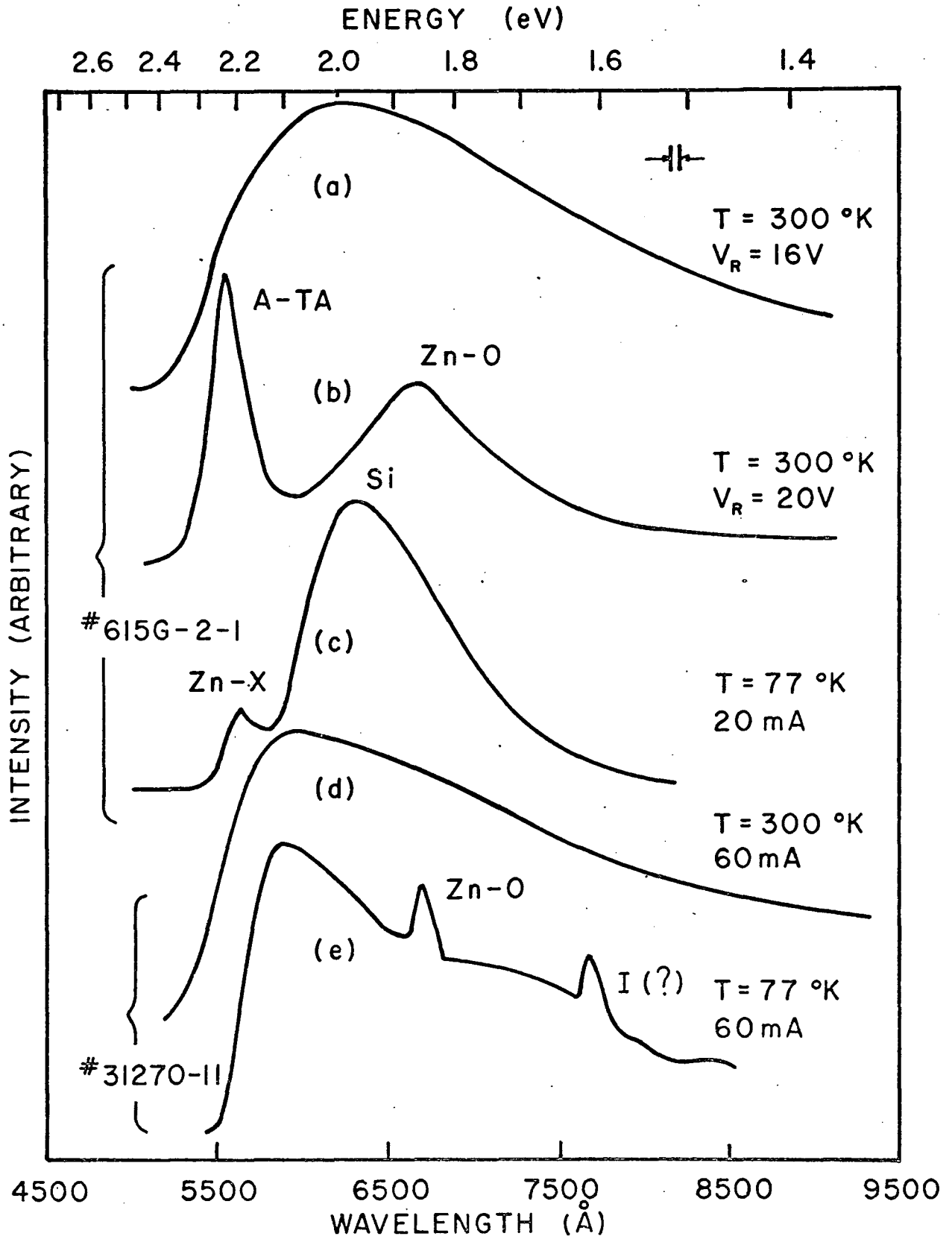
ENERGY (eV)
2.6
2.4
2.2
2.0
1.8
1.6
1.4
(a)
T = 300 °K
V_R = 16V
A-TA
Zn-O
(b)
T = 300 °K
V_R = 20V
Si
#615G-2-1
(c)
Zn-X
T = 77 °K
20 mA
(d)
T = 300 °K
60 mA
Zn-O
(e)
I (?)
T = 77 °K
60 mA
#31270-11
INTENSITY (ARBITRARY)
4500
5500
6500
7500
8500
9500
WAVELENGTH (Å)

FIGURE 16

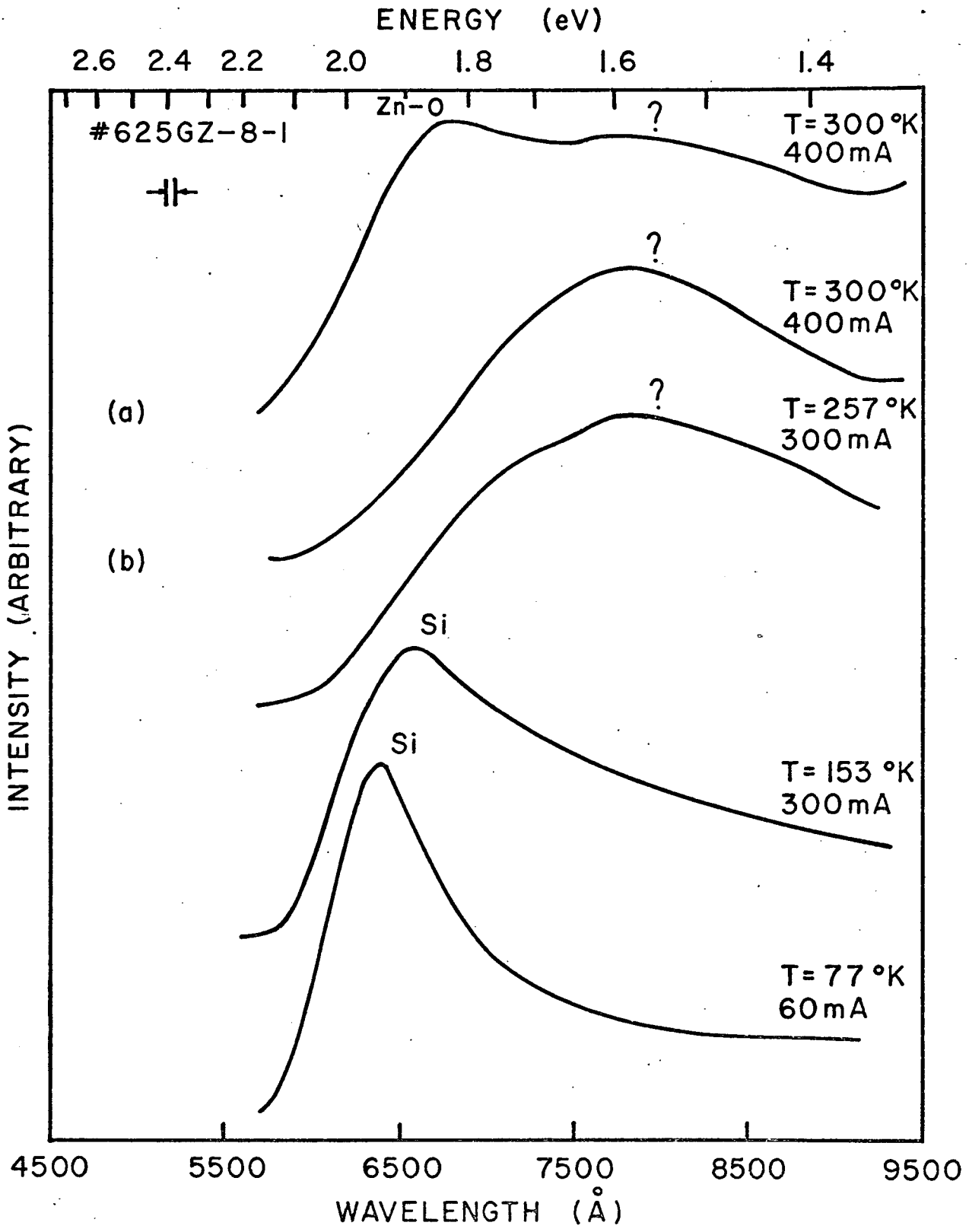
ENERGY (eV)
2.6
2.4
2.2
2.0
1.8
1.6
1.4
Zn-O
#625GZ-8-1
?
T=300°K
400mA
?
T=300°K
400mA
(a)
?
T=257°K
300mA
(b)
Si
Si
T=153°K
300mA
T=77°K
60mA
INTENSITY (ARBITRARY)
4500
5500
6500
7500
8500
9500
WAVELENGTH (Å)

FIGURE 17

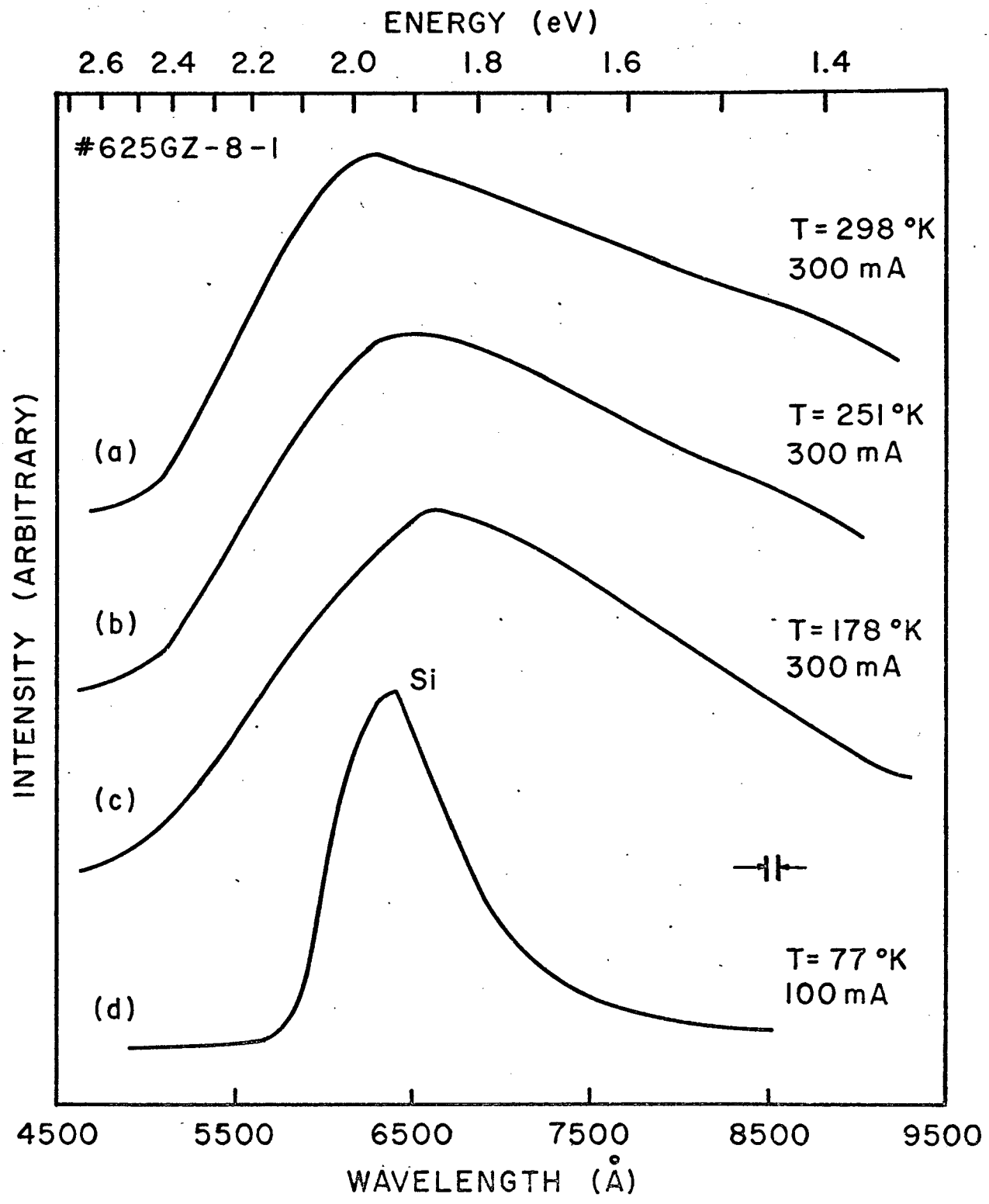
ENERGY (eV)
2.6
2.4
2.2
2.0
1.8
1.6
1.4
#625GZ-8-1
T = 298 °K
300 mA
T = 251 °K
300 mA
T = 178 °K
300 mA
T = 77 °K
100 mA
(a)
(b)
(c)
(d)
Si
INTENSITY (ARBITRARY)
4500
5500
6500
7500
8500
9500
WAVELENGTH (Å)

FIGURE 18

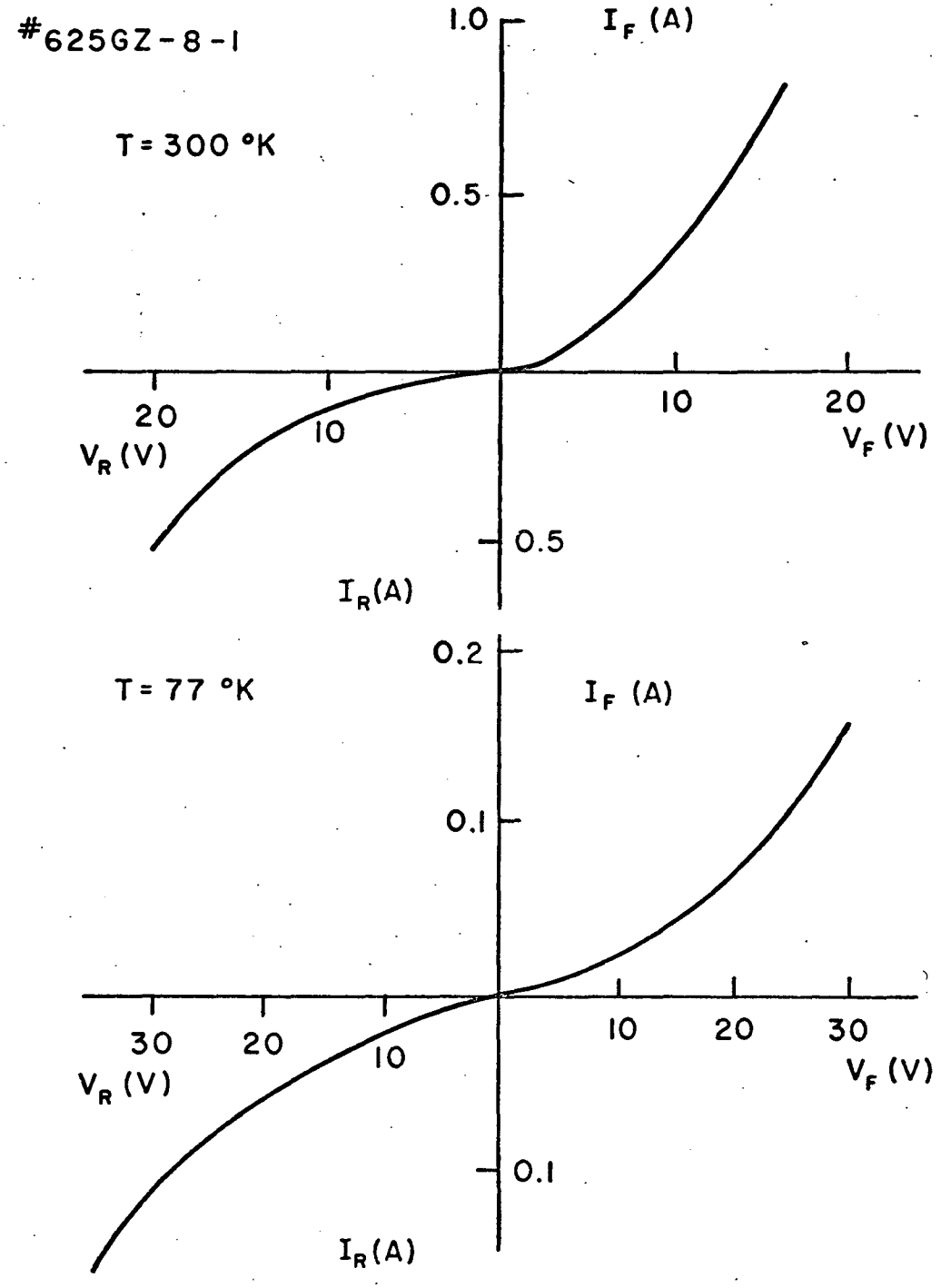
#625GZ-8-1
T = 300 °K
1.0
I_F (A)
0.5
20
10
V_R (V)
10
20
V_F (V)
0.5
I_R(A)
T = 77 °K
0.2
I_F (A)
0.1
30
20
10
V_R (V)
10
20
30
V_F (V)
0.1
I_R(A)

FIGURE 19

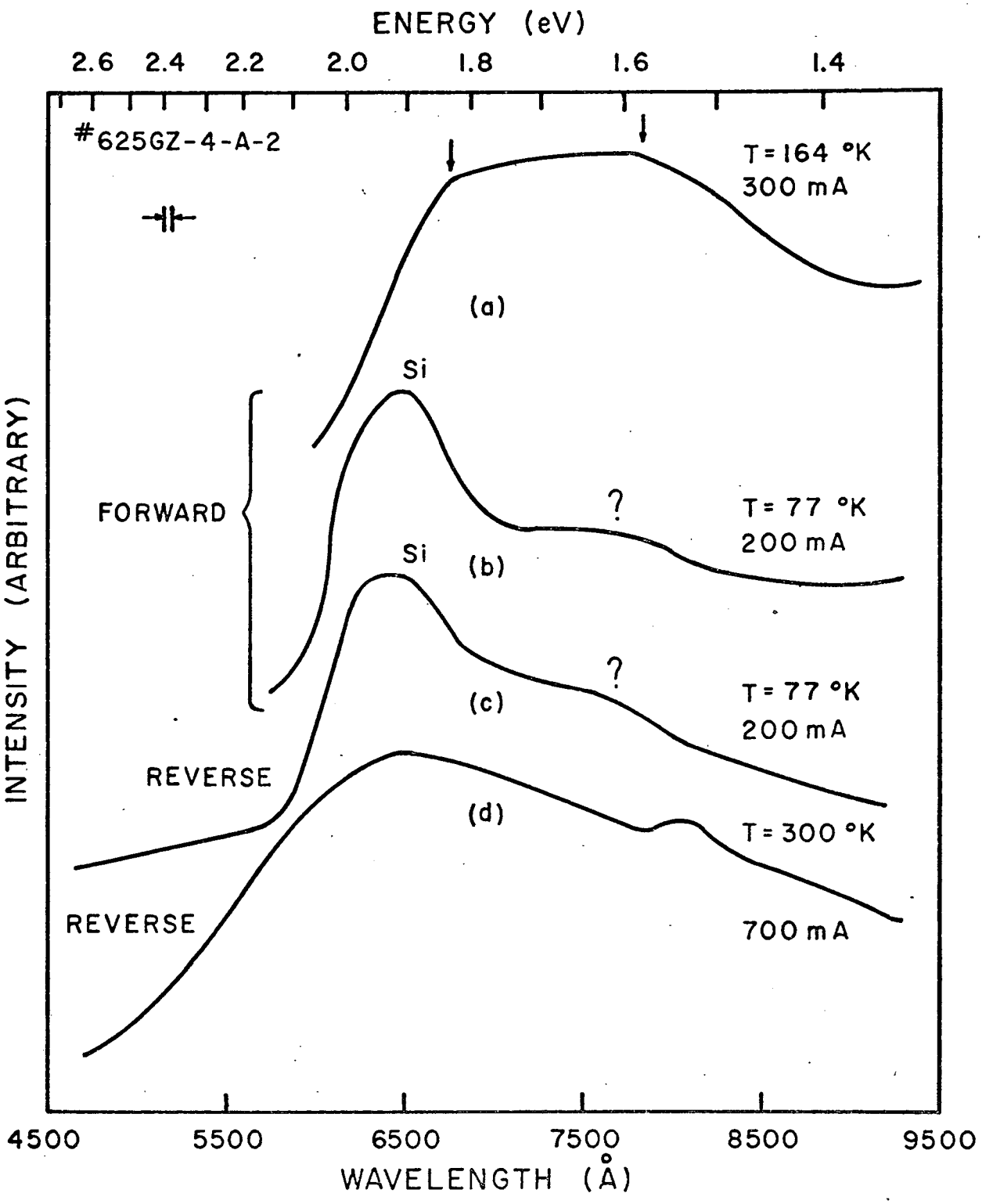
ENERGY (eV)
2.6
2.4
2.2
2.0
1.8
1.6
1.4
#625GZ-4-A-2
T = 164 °K
300 mA
(a)
Si
FORWARD
?
T = 77 °K
200 mA
Si
(b)
?
(c)
T = 77 °K
200 mA
REVERSE
(d)
T = 300 °K
REVERSE
700 mA
INTENSITY (ARBITRARY)
4500
5500
6500
7500
8500
9500
WAVELENGTH (Å)

FIGURE 20

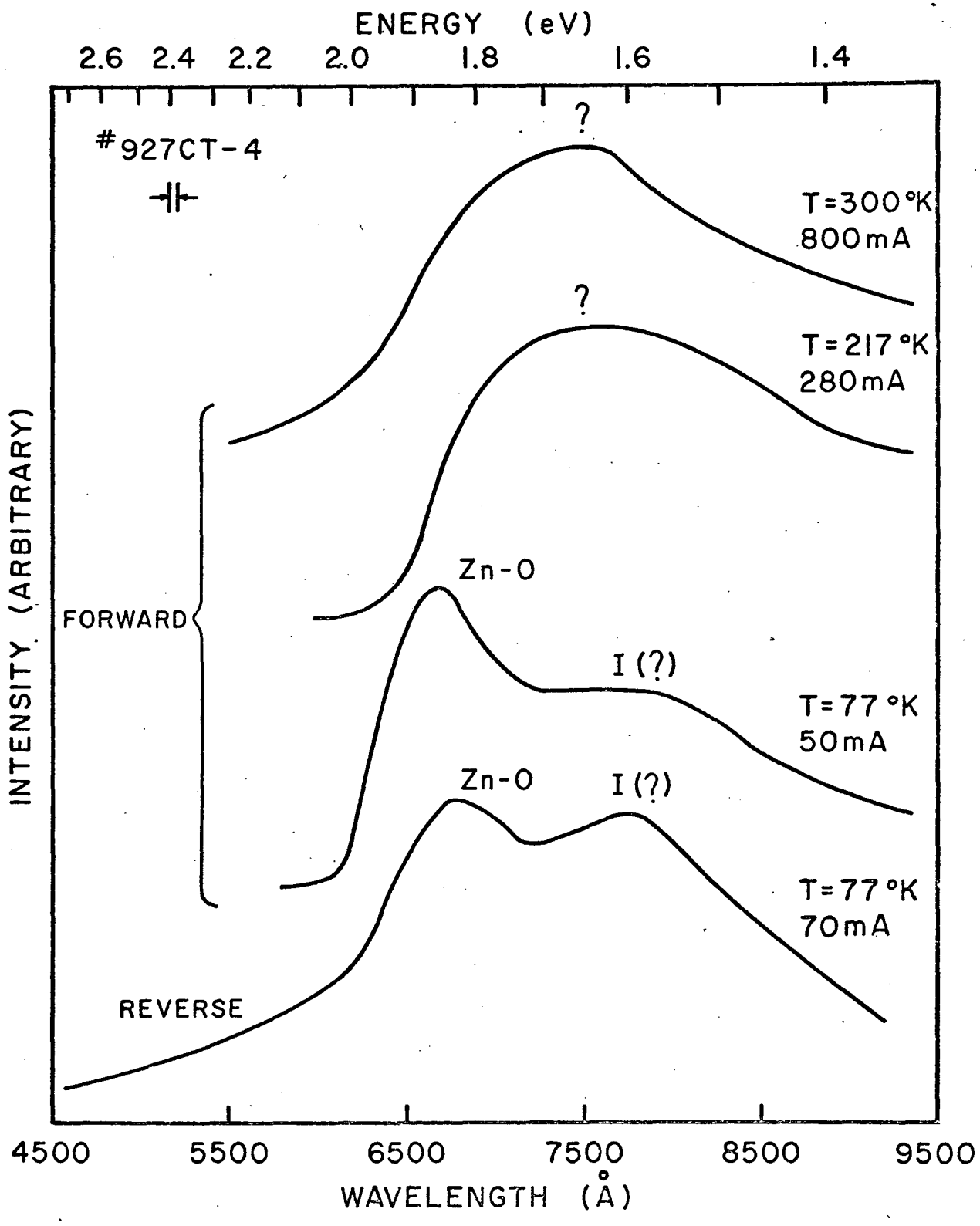
ENERGY (eV)
2.6
2.4
2.2
2.0
1.8
1.6
1.4
#927CT-4
?
T=300°K
800mA
?
T=217°K
280mA
Zn-O
FORWARD
I (?)
T=77°K
50mA
Zn-O
I (?)
T=77°K
70mA
REVERSE
INTENSITY (ARBITRARY)
4500
5500
6500
7500
8500
9500
WAVELENGTH (Å)

FIGURE 21

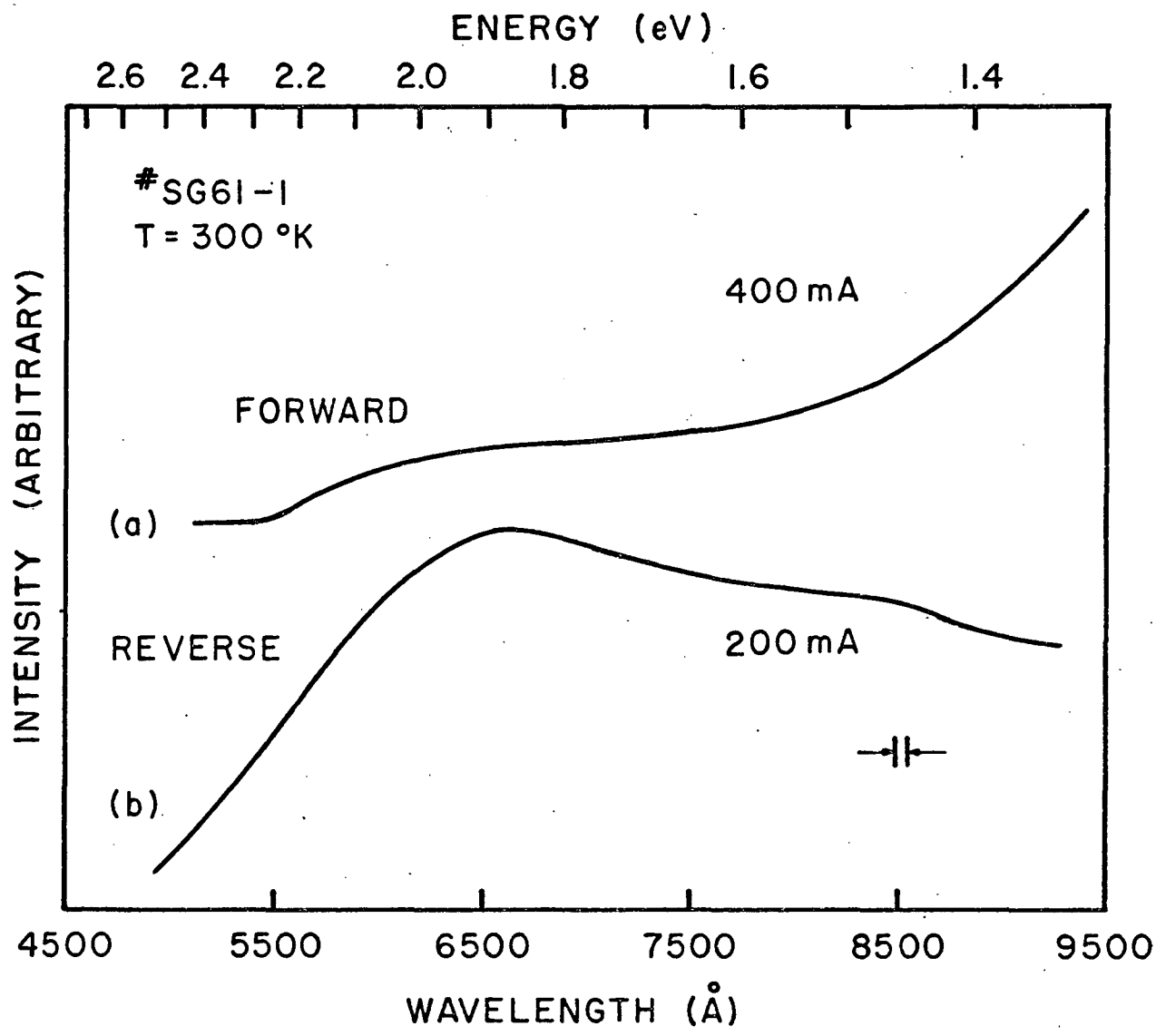
ENERGY (eV)
2.6
2.4
2.2
2.0
1.8
1.6
1.4
#SG61-1
T = 300 °K
400 mA
FORWARD
(a)
REVERSE
200 mA
(b)
INTENSITY (ARBITRARY)
4500
5500
6500
7500
8500
9500
WAVELENGTH (Å)

FIGURE 22

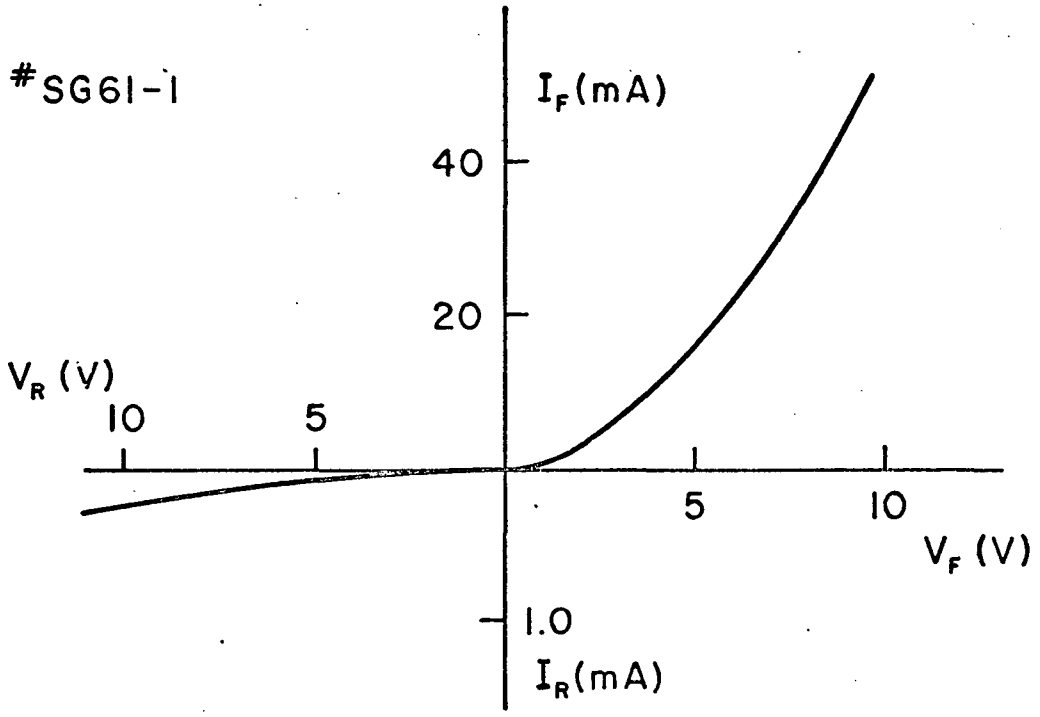

FIGURE 23

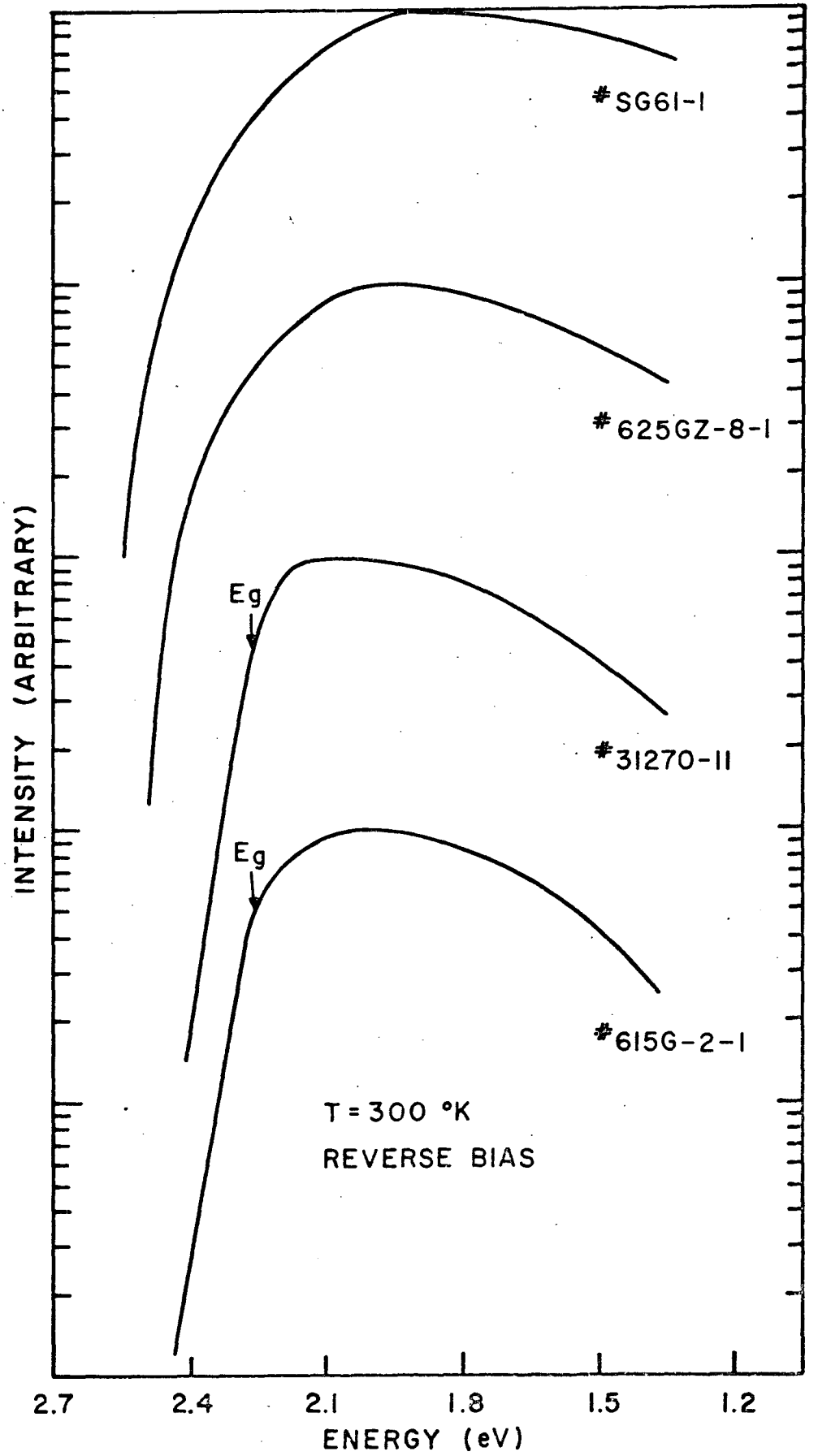
#SG61-1
#625GZ-8-1
Eg
#31270-11
Eg
#615G-2-1
T = 300 °K
REVERSE BIAS
INTENSITY (ARBITRARY)
2.7
2.4
2.1
1.8
1.5
1.2
ENERGY (eV)

FIGURE 24